OFFICE OF NAVAL RESEARCH

Contract N00014-91-J-1910

R & T Code 4131025

Technical Report #48

Substituent Effects and Bonding Characteristics in o-Benzoquinonediiminebis(bipyrdine) Ruthenium(II) Complexes

By

H. Masui, E.S. Dodsworth and A.B.P. Lever*

in

Inorganic Chemistry

York University
Department of Chemistry, 4700 Keele St., North York
Ontario, Canada M3J 1P3

REPORT DOCUMENTATION PAGE

Form Approved
OMB No 0704-0188

1 AGENCY USE ONLY (Leave blank)	2. REPORT DATE	3. REPORT TYPE AND DATES COVERED
	October 23, 1992	Technical - June 1991 to July 1992

4 TITLE AND SUBTITLE

Substituent Effects and Bonding Characteristics in o-Benzoquinonediiminebis(bipyridine)Ruthenium(II) Complexes

5. FUNDING NUMBERS

C - N00014-91-J-1910

PR - 4131025

6 AUTHOR(S)

H. Masui, E.S. Dodsworth and A.B.P. Lever*

7 PERFORMING ORGANIZATION NAME(S) AND ADDRESS(ES)

A.B.P. Lever, Department of Chemistry
York University, 4700 Keele St.
North York, Ontario M3J 1P3, Canada

8. PERFORMING ORGANIZATION REPORT NUMBER

Report #48

9 SPONSORING/MONITORING AGENCY NAME(S) AND ADDRESS(ES)

Dr. Ronald A. De Marco
Office of Naval Research, Chemistry Division
800 N. Quincy St., Arlington, VA 22217 U.S.A.

10. SPONSORING/MONITORING AGENCY REPORT NUMBER

11. SUPPLEMENTARY NOTES

12a. DISTRIBUTION/AVAILABILITY STATEMENT

12b. DISTRIBUTION CODE

13. ABSTRACT *(Maximum 200 words)*

The effect of substituents on the electrochemistry and electronic spectroscopy of $Ru^{II}(bpy)_2LL$ complexes is reported, where bpy = 2,2'-bipyridine and LL = 4,5-disubstituted o-benzoquinonediimines, o-semiquinonediimines, o-phenylenediamides and o-phenylenediamines. These data are used to create a map of the orbital energies as a function of the Hammett parameter of the substituents, giving insight into the electronic behavior of these complexes. Electronic spectra are characterized with respect to energy, intensity and bandwidth, and bands are assigned with support from resonance Raman (rR) and FTIR data. The solvatochromism of the o-benzoquinonediimine species is discussed. The data are interpreted in the context of metal-ligand orbital mixing and electronic structure. An ab initio study of the uncomplexed ligand in its quinonediimine oxidation state, is also included.

14. SUBJECT TERMS

Ruthenium, Electrochemistry, Quinone, Benzoquinonediimine, Electronic Spectra

15. NUMBER OF PAGES

44

16. PRICE CODE

17. SECURITY CLASSIFICATION OF REPORT	18. SECURITY CLASSIFICATION OF THIS PAGE	19. SECURITY CLASSIFICATION OF ABSTRACT	20. LIMITATION OF ABSTRACT
Unclassified	Unclassified	Unclassified	

TECHNICAL REPORT DISTRIBUTION LIST - GENERAL

Office of Naval Research (2)*
Chemistry Division, Code 1113
800 North Quincy Street
Arlington, Virginia 22217-5000

Dr. James S. Murday (1)
Chemistry Division, Code 6100
Naval Research Laboratory
Washington, D.C. 20375-5000

Dr. Robert Green, Director (1)
Chemistry Division, Code 385
Naval Air Weapons Center
Weapons Division
China Lake, CA 93555-6001

Dr. Elek Lindner (1)
Naval Command, Control and Ocean
Surveillance Center
RDT&E Division
San Diego, CA 92152-5000

Dr. Bernard E. Douda (1)
Crane Division
Naval Surface Warfare Center
Crane, Indiana 47522-5000

Dr. Richard W. Drisko (1)
Naval Civil Engineering
Laboratory
Code L52
Port Hueneme, CA 93043

Dr. Harold H. Singerman (1)
Naval Surface Warfare Center
Carderock Division Detachment
Annapolis, MD 21402-1198

Dr. Eugene C. Fischer (1)
Code 2840
Naval Surface Warfare Center
Carderock Division Detachment
Annapolis, MD 21402-1198

Defense Technical Information
Center (2)
Building 5, Cameron Station
Alexandria, VA 22314

* Number of copies to forward

ABSTRACT DISTRIBUTION LIST

Professor Hector Abruña
Department of Chemistry
Cornell University
Ithaca, NY 14853

Dr. Allen J. Bard
Department of Chemistry
University of Texas at Austin
Austin, TX 78712-1167

Professor Lesser Blum
Department of Physics
University of Puerto Rico
Rio Piedras, Puerto Rico 00931

Professor Daniel Buttry
Department of Chemistry
University of Wyoming
Laramie, WY 82071

Professor Richard M. Crooks
Department of Chemistry
University of New Mexico
Albuquerque, NM 87131

Professor Andrew Ewing
Department of Chemistry
152 Davey Laboratory
Pennsylvania State University
University Park, PA 16802

Professor Gregory Farrington
University of Pennsylvania
Department of Materials Science and Engineering
3231 Walnut Street
Philadelphia, Pennsylvania 19104

Professor W. R. Fawcett
Department of Chemistry
University of California, Davis
Davis, CA 95616

Dr. John J. Fontanella
Physics Department
U.S. Naval Academy
Annapolis, MD 21402-5026

Professor Harry Gray
California Institute of Technology
127-72
Pasadena, California 91125

Professor Joel Harris
Department of Chemistry
University of Utah
Salt Lake City, UT 84112

Dr. Adam Heller
Department of Chemical Engineering
University of Texas at Austin
Austin TX 78712-1062

Professor Pat Hendra
The University
Southampton SO9 5NH
England

Professor Joseph Hupp
Department of Chemistry
Northwestern University
Evanston, IL 60208

Professor Jiri Janata
Department of Bioengineering
University of Utah
Salt Lake City, UT 84102

Professor A. B. P. Lever
Department of Chemistry
York University
4700 Keele Street
North York, Ontario M3J 1P3

Professor Nathan S. Lewis
Division of Chemistry and Chemical Engineering
California Institute of Technology
Pasadena, CA 91125

Dr. Bor Yann Liaw
University of Hawaii at Manoa
2540 Maile Way, Spalding 253
Honolulu, HI 96822

Professor Rudolph Marcus
Division of Chemistry and Chemical Engineering
California Institute of Technology
Pasadena, CA 91125

Professor Charles Martin
Department of Chemistry
Colorado State University
Ft. Collins, CO 80523

Dr. Donald Maricle
International Fuel Cells
P. O. Box 739
195 Governors Highway
South Windsor, CT 06074

Dr. Melvin H. Miles
Energetic Materials Branch, Code 3853
Chemistry Division, Research Department
Naval Weapons Center
China Lake CA 93555

Professor Royce W. Murray
Department of Chemistry
University of North Carolina at Chapel Hill
Chapel Hill, NC 27514

Dr. David J. Nagel
Naval Research Laboratory
Code 4600
4555 Overlook Avenue, S.W.
Washington, D.C. 20375-5000

Dr. Michael R. Philpott
IBM Research Division
Almaden Research Center
650 Harry Road
San Jose, CA 95120-6099

Professor B. S. Pons
Department of Chemistry
University of Utah
Salt Lake City, UT 84112

Dr. Mark A. Ratner
Department of Chemistry
Northwestern University
Evanston, IL 60208

Dr. Debra Rolison
Code 6170
Naval Research Laboratory
Washington, DC 20375-5000

Dr. Michael J. Sailor
Department of Chemistry
University of California, San Diego
9500 Gilman Drive
La Jolla CA 92093-0506

Professor Jack Simons
Department of Chemistry
University of Utah
Salt Lake City, UT 84112

Professor John L. Stickney
University of Georgia
Department of Chemistry
Cedar Street
Athens, GA 30602

Professor Eric M. Stuve
Dept. of Chemical Engineering, BF-10
University of Washington
Seattle, Washington 98195

Dr. Stanislaw J. Szpak
Code 574
Naval Ocean Systems Center
San Diego, CA 92152-5000

Dr. E. Jennings Taylor
Physical Sciences, Inc.
20 New England Business Center
Andover MA 01810

Dr. Petr Vanysek
Department of Chemistry
Northern Illinois University
DeKalb, IL 60115

Professor Michael Weaver
Department of Chemistry
Purdue University
West Lafayette, IN 49707

Professor Henry S. White
Department of Chemical Engineering
and Materials Science
421 Washington Avenue, SE
University of Minnesota
Minneapolis, MN 55455

Professor R. Mark Wightman
Department of Chemistry
CB #3290, Venable Hall
The University of North Carolina
Chapel Hill NC 27599-3290

Professor George Wilson
Department of Chemistry
University of Kansas
Lawrence, KS 66045

Professor Mark S. Wrighton
Department of Chemistry
Massachusetts Institute of Technology
Cambridge, MA 02139

Professor Ernest Yeager
Case Center for Electrochemical Sciences
Case Western Reserve University
Cleveland, OH 44106

Contribution from the Dept. of Chemistry,
York University, North York (Toronto),
Ontario, Canada, M3J 1P3.

Substituent Effects and Bonding Characteristics in o-Benzoquinonediiminebis(bipyridine) Ruthenium(II) Complexes.

By Hitoshi Masui, A. B. P. Lever* and Elaine S. Dodsworth.

The effect of substituents on the electrochemistry and electronic spectroscopy of $Ru^{II}(bpy)_2LL$ complexes is reported, where bpy = 2,2'-bipyridine and LL = 4,5-disubstituted o-benzoquinonediimines, o-semiquinonediimines, o-phenylenediamides and o-phenylenediamines. These data are used to create a map of the orbital energies as a function of the Hammett parameter of the substituents, giving insight into the electronic behavior of these complexes. Electronic spectra are characterized with respect to energy, intensity and bandwidth, and bands are assigned with support from resonance Raman (rR) and FTIR data. The solvatochromism of the o-benzoquinonediimine species is discussed. The data are interpreted in the context of metal-ligand orbital mixing and electronic structure. An ab initio study of the uncomplexed ligand in its quinonediimine oxidation state, is also included.

Introduction

Quinonoid ligands[1-19] and their analogues, the o-benzoquinonediimines[20-39], are redox active species that produce complexes in which mixing between metal and ligand orbitals can play an important role in determining the physical and chemical properties of the complexes. We have been interested in studying how the electronic structures of such complexes may be probed.[4-8,18,19] When there is considerable covalency between a redox-active metal centre and a coordinated redox-active ligand, the assignment of oxidation states to the metal or to the ligand may be ambiguous. Such is the case for the o-benzoquinonediiminebis(bipyridine) ruthenium(II) complex which can be formally regarded as having a ruthenium(II) quinonoid electronic configuration but has some characteristics of a ruthenium(III) semiquinonoid species.[18,40]

The degree of covalency between the metal and ligand orbitals is a function of the energies, symmetries and overlap of the valence metal and ligand orbitals. In this study, we were interested in determining how the electronic structure is affected by a change in the energy of the o-benzoquinonediimine valence orbitals, and by a change in the net oxidation state of this ligand.

The energies of the ligand orbitals were adjusted by attaching electron donating or withdrawing substituents onto the 4 and 5 positions of the quinonoid ring. Solvatochromic studies were also carried out to provide a means of assessing the charge transfer character of the electronic transitions exhibited by these complexes. Resonance Raman (rR) and Fourier Transform Infrared (FTIR) vibrational data are also reported in support of our conclusions. The resulting shifts in the redox potentials and charge transfer bands were interpreted using a molecular orbital analysis based on that reported by Magnuson and Taube.[41] Orbital energies are mapped as a function of the Hammett $\Sigma\sigma_p$ values of the substituents, in accordance with spectroscopic assignments, transition energies and redox potentials of the complexes. We also include an ab initio study of the molecular orbital energies of the uncomplexed ligand in its quinonoid oxidation state.

The ligands in the o-benzoquinonediimine, o-semiquinonediimine and o-phenylenediamide oxidation states are designated R_2-bqdi (carrying no net charge), R_2-sqdi (carrying one negative charge) and R_2-opda (carrying two negative charges) respectively, where R denotes the substituent. The neutral o-phenylenediamine ligand is distinguished from the diamide form, where one proton has been removed from each amino group, by the abbreviations R_2-opdaH_2 and R_2-opda, respectively.

Experimental Section

Reagents

All of the commercially obtained o-phenylenediamine ligands were reagent grade or better and were used without further purification. Water was doubly distilled (the second time from potassium permanganate), and passed through Barnstead activated charcoal and ion exchange filters. Solvents were dried and distilled by standard methods just prior to use.[42]

Physical Measurements

Electronic spectra were obtained on CARY model 2400 and Hitachi-Perkin Elmer Model 340 spectrometers. Nuclear magnetic resonance (nmr) spectra were recorded on a Bruker AM300 nmr spectrometer. The observed splittings of the nmr signals are described as singlets(s), doublets(d), triplets(t), or multiplets(m). Cyclic and differential pulse voltammograms were obtained using Princeton Applied Research Corporation (PARC) 173, 174 and 179 instrumentation at platinum wire electrodes in dry acetonitrile solutions containing 0.1 M tetrabutylammonium hexafluorophosphate ($TBAPF_6$). A AgCl-coated silver wire, separated from the bulk solution by a frit, served as a quasi-reference electrode, and ferrocene was added as an internal reference. Potentials are reported versus SCE, assuming the ferricenium/ferrocene couple to be at 0.425 V vs. SCE.[43] Spectroelectrochemistry was performed either in a Hartl cell[44] or in a 1 cm glass cuvette using acetonitrile solutions containing 0.3 M $TBAPF_6$, a platinum mesh working electrode, a nichrome wire counter electrode separated from bulk by a frit, and the aforementioned quasi-reference electrode. Substituent dependence studies were carried out in acetonitrile solutions except where

otherwise stated.

Resonance Raman spectra in CH_2Cl_2 were recorded at the University of Amsterdam, using a DILOR XY resonance Raman spectrometer. These data were calibrated against solvent bands. A detailed discussion of these data, in relation to those of other similar compounds, will appear elsewhere.[45]

Ab initio calculations were performed using Spartan, (Wavefunction Inc., California) running on a Silicon Graphics Personal Iris computer. The STO3G basis set was used, and the geometry optimized at the AM1 level.

Syntheses

4,5-dimethoxy-1,2-benzenediamine monohydrochloride. The preparation of this compound has previously been reported[46], however, better yields were obtained by the following method. To a solution of 4,5-dinitroveratrole[47] (0.500 g; 2.55 mmol) in concentrated HCl (10 mL) was added $SnCl_2 \cdot 2H_2O$ (3.27 g; 14.5 mmol). The mixture was stirred, in a closed container, for 16 hr during which time the yellow solution became nearly colourless and some product precipitated from solution. Complete precipitation was achieved by saturating the reaction mixture with diethyl ether. The white, granular product was isolated by filtration, washed with 1:9 EtOH:H_2O, diethyl ether and hexanes, and air dried. The product was recrystallized from a minimum amount of 5:1 EtOH:H_2O by the rapid addition of diethyl ether. Large, white plates crystallized within 15 min and were isolated by filtration. Yield = 90% Anal: Calc'd. for $C_8H_{13}N_2O_2Cl$: C;46.92; H,6.40; N,13.74. Found: C,46.85; H,6.42; N,13.51.

$[Ru(bpy)_2(R_2\text{-}opdaH_2)](PF_6)_2$; R = OMe, Me, H, Cl. These complexes were synthesized according to the following general procedure: Dichlorobis(bipyridine)ruthenium(II)[48] (0.100 g; 0.206 mmol) was suspended in 5 ml of methanol under a nitrogen atmosphere. To the suspension was added a 10% excess (1:1 stoichiometry) of the appropriate 4,5-disubstituted o-phenylenediamine. The mixture was refluxed for 16 hr during which time the initial purple suspension was converted to a blood red solution. The solution was filtered under an inert atmosphere, and a deoxygenated solution

containing NH_4PF_6 (0.3 g) in 5% aqueous acetic acid (5 ml) was added to the filtrate. The mixture was heated briefly to boiling and then allowed to cool slowly to room temperature. The resulting crystals were isolated by quick filtration in air, washed with small amounts of ice cold water, and copious amounts of diethyl ether and hexanes, and dried in vacuo.

NMR data for the R = OMe complex in deuterated acetonitrile referenced to TMS: 3.78(6,s), 4.79(2,d), 5.43(2,d) 6.80(2,s), 7.20(2,t), 7.63(2,t) 7.69(2,d), 7.84(2,t), 8.13(2,t) 8.34(2,d), 8.50(2,d), 8.71(2,d).

$[Ru(bpy)_2(R_2\text{-bqdi})](PF_6)_2$; R = Cl, H, and Me. The synthetic procedure for the corresponding R_2-opdaH_2 complexes was followed until the blood-red solution was obtained. After cooling, concentrated ammonia (1.0 mL) was added to the solution and the mixture was bubbled with air until all of the solvent evaporated. The exposure to air deepens the colour of the solution. The residue was redissolved in the minimum amount of methanol and NH_4PF_6 (0.3 g) was added slowly to the solution as an aqueous solution of equal volume. The resulting precipitate was isolated, rinsed with ice water, copious amounts of diethyl ether and hexanes. Recrystallization was achieved by slowly cooling a hot, saturated, aqueous solution of the product.

$[Ru(bpy)_2(R_2\text{-bqdi})](PF_6)_2$; R = NH_2 and OMe. 1,2,4,5-benzenetetraamine tetrahydrochloride (Aldrich) was used in the synthesis of the diamino-substituted complex while 4,5-dimethoxy-1,2-benzenediamine monohydrochloride (vide supra) was used in the synthesis of the dimethoxy-substituted complex. One equivalent of sodium acetate dihydrate per hydrochloride of ligand was added, in a nitrogen atmosphere, to a mixture containing dichlorobis(bipyridine)ruthenium and 10% excess (1:1 stoichiometry) of ligand in methanol (5 mL) to generate the neutral, free ligand in situ. Following the formation of a blood-red solution, the procedure was then continued as above.

The diamino-substituted complex was purified by soxhlet extraction of the crude solid with dichloromethane. As the extract became concentrated, it yielded fine crystals of the product.

NMR data for R = NH_2 complex in deuterated acetone, referenced to TMS: 6.20(s,6), 7.49(t,2), 7.75(t,2), 7.84(d,2), 8.08(t,2), 8.21(t,2), 8.39(d,2), 8.70(t,4), 10.46(s,2).

NMR data for the R = OMe complex in deuterated acetonitrile referenced to TMS: 3.84(6,s), 6.40(2,s), 7.41(2,t) 7.56(4,m), 7.90(2,d), 8.03(2,t) 8.11(2,t), 8.21(4,d), 10.94(2,s).

$[Ru(bpy)_2(NO_2\text{-}bqdi)](PF_6)_2$. (N.b. the NO_2 substituted ligand is mono-substituted in the 4 position whereas all other ligands are di-substituted in the 4 and 5 positions). To a suspension of dichlorobis(bipyridine)ruthenium(II) (0.1g; 0.206 mmol) in methanol (5 ml) was added silver nitrate (0.070 g; 0.412 mmol). The mixture was stirred for 3 hr and then filtered through a Celite bed. The blood-red filtrate was deoxygenated, placed under a nitrogen atmosphere, and treated with 4-nitro-1,2-benzenediamine (0.035 g; 0.228 mmol). The mixture was refluxed for 16 hr and subsequently filtered. The filtrate was bubbled with air until the solvent evaporated. The resulting residue was further purified by chromatography on a silica column, eluting with a mixture containing 1:1 acetone:water and 1% w/v KCl. The largest fraction was collected and concentrated, and the product was precipitated by the addition of NH_4PF_6.

$[Ru(bpy)_2((NH_2)_2\text{-}opdaH_2)](PF_6)_2$ This complex was obtained by treating a saturated solution of the $(NH_2)_2$-bqdi complex in 10% aqueous acetic acid with zinc amalgam powder under an inert atmosphere. The solution was filtered to remove excess zinc amalgam and the product was precipitated from the resulting orange-red filtrate by adding an excess of NH_4PF_6. Microcrystals were isolated by filtration under nitrogen and washed with small amounts of cold 10% acetic acid and copious amounts of diethyl ether, and dried in vacuo.

N.b. Sodium perchlorate (0.3 g) was used instead of NH_4PF_6 in some of the earlier syntheses and seems to produce better quality crystals but the practice was discontinued for safety reasons.

Although the R_2-bqdi and R_2-opdaH_2 species were directly prepared and obtained as solid materials, the R_2-sqdi species were not isolated due their rapid oxidation in air. The spectroelectrochemical data for the R_2sqdi species were obtained by controlled potential

reduction of the R_2-bqdi species at a potential 100 mV negative of the first reduction wave.

Chemical Analyses.

$[Ru(bpy)_2(bqdi)](PF_6)_2$ Anal. % Calcd for $C_{26}H_{22}F_{12}N_6P_2Ru$:
C, 38.58; H, 2.74; N, 10.38. % Found: C, 38.78; H, 2.90; N, 10.10.

$[Ru(bpy)_2((NH_2)_2\text{-bqdi})](PF_6)_2 \cdot H_2O$ Anal. % Calcd for $C_{26}H_{26}F_{12}N_8OP_2$ Ru:
C, 36.42; H, 3.06; N, 13.07. % Found: C, 36.11; H, 2.91; N, 12.52.

$[Ru(bpy)_2((CH_3)_2\text{-bqdi})](PF_6)_2$ Anal. % Calcd for $C_{28}H_{26}F_{12}N_6P_2$ Ru:
C, 40.15; H, 3.13; N, 10.03. % Found: C, 40.24; H, 3.44; N, 10.03.

$[Ru(bpy)_2(Cl_2\text{-bqdi})](PF_6)_2$ Anal. % Calcd for $C_{26}H_{20}Cl_2F_{12}N_6P_2Ru$:
C, 35.55; H, 2.29; N, 9.57. % Found: C, 35.47; H, 2.65; N, 9.47.

$[Ru(bpy)_2((OCH_3)_2\text{-opdaH}_2)](ClO_4)_2$. Anal. % Calcd for $C_{28}H_{26}Cl_2N_6O_{10}Ru$:
C, 43.20; H, 3.37; N, 10.79. % Found: C, 43.02; H, 3.49; N, 10.68.

$[Ru(bpy)_2(NO_2\text{-bqdi})](PF_6)_2$ Anal. % Calcd for $C_{26}H_{21}F_{12}N_7O_2P_2Ru$:
C, 36.55; H, 2.48; N, 11.47. % Found: C, 37.31; H, 2.76; N, 11.75.

Summary of Resonance Raman spectra. Data collected in dichloromethane solution, peak energies in cm^{-1}, relative intensities in brackets: $[Ru(bpy)_2(Cl_2\text{-bqdi})]^{2+}$ Excitation at 543 nm:-310(0.13); 491(0.12); 601(1.0); 656(0.21); 669(0.25); 916(0.087); 1200,1218(0.17); 1264(0.11). $[Ru(bpy)_2(Cl_2\text{-sqdi})]^{+}$ Excitation at 515 nm:- 604 (bqdi impurity); 665,672(0.8); 1169(0.52); 1263(0.35); [1314(0.39)]; 1484(1.0); [1517(0.52)]; 1557(0.52); 1604(0.2). Peaks in square brackets were not observed in all run of this species and may arise from decomposition products. Excitation at 620 nm:-570(1.0); 666(0.3); 819(0.1); 1140(0.16); 1195(0.41); 1352(0.23); 1477(0.35) cm^{-1}.

Summary of ν(Ru-N) FTIR data. Data collected using KBr pellets. Peak energies in cm^{-1}: R = NO_2 (mono-substituted in the 4-position, chloride salt), 556; R = Cl, 599; R = H, 620; R = Me, 603; R = OMe, 594; R = NH_2, 591 cm^{-1}

Results and Discussion

A. Molecular Orbital Energy Level Diagram

In the discussion which follows, symmetry labels appropriate to the local C_{2v} point group are used. Ab initio calculations of the free ligand fragment show that the HOMO π level has a_2 symmetry (labelled a_2) and lies approximately 10,000 cm^{-1} above the SHOMO (second highest occupied MO) which is σ or π depending upon substituent (Table I). The LUMO π^* has b_2 (labelled $2b_2^*$) symmetry. As discussed previously,[4,18] group theoretical methods lead to the simplified molecular orbital diagram (Figure 1), appropriate for the bqdi and sqdi oxidation states. The HOMO (π) and LUMO (π^*) of the bqdi ligand will couple to the metal (xy) $2a_2$ and (yz) b_2 orbitals respectively, with the latter interaction being more important than the former due to a more favorable overlap. The remaining $d(t_{2g})$ orbital is (z^2) a_1 (in this framework, see Figure 1, orbitals rotated with axes) and has some σ^* character from interaction with the low lying bqdi $9a_1$ orbital. The data below lead to the conclusion that the a_1 and $2a_2$ orbitals lie close together; for the purpose of the ensuing discussion they will be assumed to be of roughly equal energy. No evidence was observed for any transitions to the next higher (2nd) LUMO of the bqdi or sqdi species.

B) Electrochemistry.

The cyclic voltammogram of a R_2-bqdi complex, displayed in Figure 2, shows five reversible or quasi-reversible ($i_a = i_c$) coulometrically determined one-electron redox processes. These were assigned previously[18,26] as shown in Table II. The two most negative processes (V,IV) correspond to the successive reduction of the bipyridine ligands; these have potentials only slightly dependent on the bqdi substituent.

The next three processes (III,II,I) formally correspond with R_2-sqdi/R_2-opda, R_2-bqdi/R_2-sqdi and Ru^{III}/Ru^{II}. The potentials of these couples all depend upon the Hammett $\Sigma\sigma_p$ parameter of the bqdi substituent, as shown in Figure 3. All of the potentials become more positive as the electron-withdrawing ability of the substituent increases. Since the substituents are each both para and meta to quinonoid nitrogen donor atoms, we used a sum of

the σ_p values for the R substituent.[49]

Indeed there is quite a large change in the donor character of the quinonoid ligand over this series of substituents. This is recognized from the values of the electrochemical parameter, E_L, for these species,[50] derived from the Ru^{III}/Ru^{II} potentials listed in Table II. These range from 0.38 for R = NO_2, similar to a phosphite, to 0.01 for R = NH_2, similar to a saturated amine. The electrochemistry of the opdaH_2 species exhibit irreversible redox processes with unusual features which will be discussed elsewhere.[51]

C. **Electronic Spectra.**

The electronic spectral data and band assignments for all complexes discussed in this paper are listed in Table III.

1) o-Benzoquinonediimine species, $[Ru(bpy)_2(R_2\text{-bqdi})]^{2+}$.

The spectrum of a typical bqdi complex shows three low energy charge transfer bands (Figure 4) whose assignments have been discussed.[18] **Band 3** usually appears as a shoulder of moderate intensity (ϵ = 5000 - 8000 cm^{-1} M^{-1}) on the high energy side of **Band 4** and its peak is resolved in complexes having more strongly electron withdrawing substituents. It lies in a region where the rR spectrum of the related $[Ru(bpy)_2(o\text{-benzoquinone})]^{2+}$ complex[8] confirms the Ru --> $\pi^*(1)$ bpy transition to occur. Further evidence for this assignment comes from the previously described relationship between the Ru^{III}/Ru^{II} redox potential and the energy of this transition, specifically,[52]

$$h\nu[Ru \rightarrow \pi^*(1)bpy] = 0.65\, E[Ru^{III}/Ru^{II}] + 2.0\ (eV) \qquad (1)$$

This relationship is expected if the HOMO, which is involved in the redox process, is also the orbital from which the charge transfer transition originates. The HOMO, in this case, is either the a_1 or $2a_2$ level since the b_2 should be stabilized below the former by strong interactions with the bqdi ligand. Using equation (1) and couple I (Table II), there is a good agreement between observed and calculated energies of this transition; thus, **Band 3** is specifically assigned to Ru $a_1,2a_2$ --> $\pi^*(1)$ bpy. The Ru $1b_2$ --> $\pi^*(1)$ bpy transition must occur at an energy that ranges from 3000 to 8000 cm^{-1} higher than that of the Ru $a_1,2a_2$ -->

$\pi^*(1)$ bpy transition. This value is estimated by subtracting the energy of **Band 5** (assigned below) from that of **Band 4**. Such a transition has not been observed but may be hidden beneath stronger, adjacent bands.

A transition from the metal to a second bipyridine orbital, $\pi^*(2)$ bpy, occurs at an energy that is approximately 8,000 cm^{-1} higher than that of **Band 3** and is often obscured by the base of an intense ligand centered π --> π^* transition. The Ru --> $\pi^*(2)$ bpy transition, labelled **Band 2**, is best resolved in the complexes having strongly electron donating substituents and can be used to estimate the energy of the $a_1,2a_2$ --> $\pi^*(1)$ bpy transition when the latter is poorly resolved.

Band 4 is assigned to a transition from the b_2 to the $2b_2^*$ LUMO of the complex[18] on the basis of its relatively high intensity, given that transitions from a_1 or $2a_2$ will be weak due to poor overlap. Resonance Raman excitation profiles plotted for the 599 cm^{-1} (R = 4,5-Cl_2) and the 620 cm^{-1} (R = H) vibrations, show that there is only one electronic transition within the envelope of **Band 4**. Although isotopic substitution is needed to unequivocally identify this vibration, it is very likely to have considerable ν (Ru-N) character.[53] Higher frequency vibrations, e.g. bqdi or bipyridine ligand C=C and C=N, are not enhanced (Figure 5).

Since the intensity of an enhanced vibration is proportional to the square of the displacement and the square of the frequency of the vibration, ie.

$I_i \propto \Delta_i^2 \omega_i^2$,

the lack of significantly enhanced vibrations near 1000 - 1600 cm^{-1}, where C=C and C=N stretches occur, provides strong evidence that their displacements are very small compared with that of the lower frequency Ru-N (diimine) stretch. Thus **Band 4** has very little charge transfer character and is essentially a transition localized in the Ru - N (diimine) bond; i.e. a π --> π^* transition involving this bond.

Band 4, which is unusually narrow, is skewed Gaussian[54] in shape, being 30 - 50% broader on the high energy side, probably due to vibronic coupling and to overlap with the adjacent **Band 3**. For discussion purposes, the bandwidth at 1/e height of this transition was

obtained by doubling the measured half-bandwidth at 1/e height from the centre of the band to lower energy.

It is not clear whether **Band 5** comprises one or two transitions but in some instances the shape of the band suggests the presence of two transitions of similar energy (Figure 4). The band is very weak, and by analogy to the assignments given for the spectrum of $[Cl(NH_3)_4Os(Hpz)]^{2+}$ by Magnuson and Taube,[41] is assigned to the symmetry allowed but overlap-forbidden transitions Ru $a_1,2a_2$ --> $2b_2^*$ (LUMO) metal to ligand charge transfer (MLCT).

a) Substituent Dependence.

The energies of **Bands 3, 4** and **5** are all dependent upon the bqdi substituent as shown in Table III and Figure 6. Generally, as the substituent becomes more electron-withdrawing **Band 3** blue shifts and **Band 5** red shifts, both to a significant degree and both linearly with respect to the Hammett $\Sigma\sigma_p$ parameter. In acetonitrile solutions, **Band 4** follows a non-linear dependence with a much smaller variation. Specifically, the energy of **Band 4** increases with $\Sigma\sigma_p$ from diamino ($\Sigma\sigma_p$ = -1.32; E = 18,100 cm^{-1}) to unsubstituted ($\Sigma\sigma_p$ = 0.00; E = 19,450 cm^{-1}) but falls as $\Sigma\sigma_p$ becomes even more positive as, for example, the nitro substituent ($\Sigma\sigma_p$ = + 0.78; E = 19,000 cm^{-1}). The bandwidth of **Band 4** generally increases with $\Sigma\sigma_p$, however, the data points deviate from the best fit line in such a way that the deviations parallel the peculiar substituent dependence of the transition energy (see further discussion below).

In aqueous acidic media, the amino groups in the R = NH_2 species can be protonated, causing **Bands 3** and **4** to blue shift, while **Band 5** red shifts (Table III). A sigmoidal titration curve (Figure 7) of the absorption intensity of **Band 4** as a function of pH allows one to estimate the pK_a value of the complex; it is found to be 0.52±0.1.

In 50% sulfuric acid the spectrum is further shifted and the complex is now apparently di-protonated. Certainly, a fit of the band energies to $\Sigma\sigma_p$ is excellent for all three transitions if diprotonation is assumed, and hence a value of $\Sigma\sigma_p$ = 1.2 is then accorded to the substituents on this species.[49]

Data are also reported for the monoprotonated species recorded in 3M aqueous HCl. The energies of **Bands 3, 4, 5** also fit the substituent dependence line fairly well assuming $\Sigma\sigma_p$ = -0.06 for the sum of NH_2 and NH_3^+, with slight deviations probably due to the aqueous solvent (Figure 6).

b) Solvatochromism.

The diamino and dichloro substituted complexes, having substituents at the near extremes of the experimentally obtained $\Sigma\sigma_p$ values, show similar solvent dependences of their charge transfer bands (Table IV). The energy of **Band 3** correlates linearly with the donor number of the solvent, DN,[55] red shifting as DN increases (4,5-Cl_2: slope = -56 cm^{-1}/DN; regression coefficient (R) = 0.96, 4,5-$(NH_2)_2$: slope = -32 cm^{-1}/DN; R = 0.97). This result indicates that charge is donated from the solvent to the benzoquinonediimine end of the complex, possibly through hydrogen bonding to the imine protons of the quinonoid ligand.

As shown by the slopes of the linear correlations, the solvent sensitivity of **Band 3** is greater for the dichloro complex than the diamino complex. This may be due to the reduced hydrogen-bonding acidity of the Cl_2-bqdi ligand at the imine protons of the diamino complex, causing weaker hydrogen bonding interactions of the protons with the solvent. It is also possible that the amine substituents of the diamino complex donate electron density directly to the solvent but this is a minor contributing factor since there are no clear correlations with solvent hydrogen bonding acidity.

Band 4 tends to shift to lower energies as the donor number of the solvent increases; however, the range of the shift is smaller than for **Band 3** and does not correlate well with DN. (4,5-Cl_2: slope = -12 cm^{-1}/DN, R = 0.78; 4,5-$(NH_2)_2$: slope = -4.9 cm^{-1}/DN; R = 0.47). This is consistent with the conclusion that **Band 3** has significant MLCT character while **Band 4** has virtually no charge transfer character.

The errors in determining the peak maxima of **Band 5** were large relative to the solvatochromic shifts; thus, for the dichloro complex it was difficult to ascertain whether **Band 5** correlates with DN. Such shifts could not be studied for the diamino complex because **Band 5** is

obscured by **Band 4.**

2) o-Semiquinonediimine species, $[Ru(bpy)_2(R_2\text{-sqdi})]^+$.

Controlled potential reduction some 100 mV negative of couple II, yields solutions of the R_2-sqdi species whose electronic spectra are reported in Table III and Figure 4. This reduction process shows Nernstian behavior for the $[Ru(bpy)_2(Cl_2\text{-bqdi})]^{2+}$ complex as is demonstrated by spectro-electrochemistry at various applied potentials through the redox wave,[56] and it is expected that the other complexes will exhibit similar behavior with the exception of the R = OMe and R = NH_2 species. These latter species undergo decomposition once a certain concentration of the R_2-sqdi species is generated.

Band 7, assigned to Ru $a_1,2a_2$ --> $\pi^*(2)$ bpy, shifts with substituent roughly parallel to the Ru $a_1,2a_2$ --> $\pi^*(1)$ bpy transitions of **Bands 8**. The transitions of **Bands 8** are well separated in the species where R = OMe, Me, and H but are overlapping or poorly resolved for R = Cl or NO_2. The substituent dependence for **Bands 8** is shown versus the Hammett $\Sigma\sigma_p$ in Figure 8.

Resonance Raman spectra were recorded for R = Cl, in regions close to the **Bands 8** and **Band 9**, the Ru b_2 --> $2b_2^*$ transition (see Expt.). Data for excitation close to **Bands 8** show the characteristic vibrational fingerprint of a Ru --> $\pi^*(1)$ bpy MLCT transition[8,57] (bands at 670, 1169, 1263, 1314, 1484 and 1557 and 1604 cm^{-1}). These bands are absent from the spectrum obtained with excitation close to **Band 9.** Instead skeletal modes of the sqdi ligand appear at 1475, 1351 and 1200 cm^{-1}, together with a strong band at 566 cm^{-1} which likely involves ν(Ru-N) (sqdi). The relatively strong enhancement of the skeletal modes, with respect to the Ru - N stretching mode typifies significant charge transfer in this transition[8]. Furthermore, **Band 9** behaves as an MLCT transition, generally shifting to the red with increasing acceptor character of the substituent.

Band 10, an ill defined weak and broad transition centered near 900 nm, may be analogous to the forbidden Ru a_1,a_2 --> $2b_2^*$ transition (**Band 5**) in the bqdi oxidation state.

3) Diamine oxidation state species, $[Ru(bpy)_2(R_2\text{-}opdaH_2]^{2+}$.

Since the diamine ligand has no low lying empty π^* orbitals, no charge transfer transitions involving the ligand and the metal are observed in the visible region. The visible absorption spectrum is then dominated by two Ru --> bpy bands, **Band 12** (Ru $a_1,2a_2$ --> π^*(2)bpy) and **Band 13** (Ru $a_1,2a_2$ --> π^*(1) bpy) (Figure 4). The dependence of **Band 13** on the Hammett $\Sigma\sigma_p$ value is shown in Figure 8. Additionally, there is a π --> π^* transition (**Band 11**) of the bipyridine ligands in the UV region which has been omitted from Figure 4 for clarity.

These data were obtained from samples of the isolated diamine complexes. Controlled potential reduction of the bqdi species in aprotic solvents negative of the sqdi/opda redox couple, yields the diamide versions of these species for R = NO_2 and to some extent, with slow decomposition, the R = Cl and R = Me species. With the softer diamide ligand, the Ru $a_1,2a_2$ --> π^*(1) bpy (**Band 16**) and the Ru $a_1,2a_2$ --> π^*(2) bpy (**Band 15**) transitions shift to the red, relative to the other $opdaH_2$ species, even though the 4-NO_2-opda and 4,5-Cl_2-opda ligands contain acceptor groups.

Consideration of the data shown in Figure 8, where the Ru --> π^*(1) bpy transition energy is plotted against $\Sigma\sigma_p$ for each oxidation state of the orthophenylene ligand, shows that this transition is strongly dependent upon substituent in both the bqdi and sqdi oxidation states, but much less so in the fully reduced $opdaH_2$ state. Evidently in this last case, the sp^3 hybridized NH_2 groups interrupt the π-conjugation of the ruthenium atom with the ligand. The marked dependence for the sqdi oxidation state demonstrates that even though these systems are believed to be less mixed than the bqdi oxidation state, the π-back-donation is still substantial.

D. **Bonding Description**

Recently Carugo et al.[40] analyzed the metal-nitrogen bond lengths of a large range of o-phenylenediamine complexes as a function of their oxidation state. They noted that these species do not generally yield charge localized structures and therefore cannot be characterized as having a formal oxidation state but rather a state between two of the three possibilities. They

argued that it is possible to identify the net oxidation state of such a species from an analysis of the deviation of all the bond lengths from standard bond lengths for the opdaH_2 and bqdi ligands. In this manner, they characterized the [Ru(bpy)$_2$(H_2-bqdi)](PF_6)$_2$ species, whose structure is known,[26] as effectively containing Ru^{III} bound to the sqdi anion. For clarity of discussion, we will refer to this species as formally containing the bqdi ligand and most of the discussion which follows refers specifically to the bqdi oxidation state, except where specific reference to the other oxidation states is made.

The behavior of these bqdi complexes may be understood on the basis of essentially 50:50 metal-ligand mixing in the b_2 and $2b_2^*$ orbitals and less mixing in the a_1 and $2a_2$ orbitals such that the latter may be considered primarily metal in character. This model is consistent with the MLCT substituent behaviour of **Band 5** (Ru a_1,$2a_2$ --> $2b_2^*$) as it shifts to lower energy with stronger acceptor groups (Figure 6). Further, the model is compatible with the blue shift of **Band 3** (Ru a_1,$2a_2$ --> π^*(1) bpy) with increasing acceptor character of the bqdi ligand (Figure 6), and with the lack of substituent dependence of **Band 4** (b_2 --> $2b_2^*$) since the orbitals involved have a mixed molecular orbital description.

a) Mapping of orbital energy levels with $\Sigma\sigma_p$ (Figure 9, Table V).

One may roughly map the molecular orbital energies in the bqdi oxidation state species as a function of Hammett $\Sigma\sigma_p$ values by using experimentally obtained transition energy data. Such a map, however, neglects configurational interaction and includes reorganization energies and is, therefore, not a precise MO picture, but these effects should be reasonably independent of substituent for a given transition, and trends in the orbital energies should be fairly accurate.

Thus, Figure 9 is constructed in the following manner. The redox process corresponding to the bipyridine reduction, couple IV, has essentially no dependence upon the bqdi substituent; thus, the π^*(1) bpy orbital can be used as an internal marker against which all other orbital energies may be referenced. The a_1,$2a_2$ levels (assumed degenerate) of the parent bqdi species (R = H) are assigned an energy of zero. These levels shift in concert with **Band 3**, the Ru a_1,$2a_2$ --> π^*(1) bpy transition. Adding the energy of **Band 5** to the a_1,$2a_2$ levels yields the

energy of $2b_2^*$. Subtracting the energy of **Band 4** from the $2b_2^*$ level, yields the energy of b_2, while subtracting the energy of the bqdi π - π^* transition from that of $2b_2^*$ yields, approximately, the energy of a_2.

The substituent dependencies for the first oxidation and the first reduction potentials should be related to those in Figure 9 since they involve the a_1,$2a_2$ and $2b_2^*$ orbitals respectively. However redox potentials describe the total free energy change in the redox process, i.e. a sum over all orbitals. The substituent dependence of this energy change will be largely determined by that of the orbital primarily involved in the redox process but must, for a metal centred process, for example, also involve other metal orbitals, especially valence orbitals of comparable energy.

The open squares on the $2b_2^*$ line in Figure 9 show the variation of couple II as a function of $\Sigma\sigma_p$, setting the species with R = H to fit onto the $2b_2^*$ line. There is a good correspondence between the two slopes, though that of the redox potential is slightly larger, probably due to a contribution from the substituent dependence of the b_2 orbital which is greater than that of $2b_2^*$.

The substituent dependence of couple I is also shown in Figure 9, normalized to a potential of zero for R = H. Its slope is considerably greater than that of the a_1,$2a_2$ line, being 2900 $cm^{-1}/\Sigma\sigma_p$ compared with 1630 $cm^{-1}/\Sigma\sigma_p$ for a_1,$2a_2$. This difference can be explained by contributions from the other valence orbitals to the substituent dependence of the redox potential. For example, averaging the slopes of the a_1,$2a_2$, and b_2 levels predicts a redox potential slope of 2410 $cm^{-1}/\Sigma\sigma_p$, closer to that observed. This value would be further increased by a contribution from the $2b_2^*$ dependence.

Comparisons of this type may help to clarify the electronic structures of these species, but they are simplified in the sense that one cannot necessarily assume that the ordering of the d orbitals, or identity of the HOMO is the same in the Ru^{III} species as it is in the Ru^{II} species; thus it may not be meaningful to talk of a redox process involving removal of an electron from a specific orbital.

The almost parallel dependence of b_2 and $2b_2^*$, following from the relatively small dependence of **Band 4** upon $\Sigma\sigma_p$, implies considerable mixing between the ruthenium d(yz) and ligand π^* orbital (back-donation). Numerical assessment of the degree of mixing, based upon earlier treatments by Vlcek,[58], de la Rosa et al.[59] and Hupp et al.[60] indicates essentially 50:50 mixing of ligand and metal orbital, when ligand and metal redox processes behave in a parallel fashion upon a perturbation such as variation of substituent. However, such treatments are approximate and are only strictly applicable where the mixing is small.

The essentially parallel dependence of the $1a_2$, $1b_2$ or $2b_2^*$ orbital energies (Table V) may be fortuitous. The $1a_2$ orbital's lower energy and lower polarizability should cause the orbital to be less substituent dependent than the $2b_2^*$ orbital, while its lesser degree of mixing with the metal, compared with $2b_2^*$, should have the opposite effect. The sum of these two effects has probably resulted in the parallel dependence of these three orbitals.

b) Reorganization energy contributions - **Band 5**

For a MLCT transition in a general complex, $M^{II}X_5L$, one may write[52]:

$$h\nu = E[M^{III}/M^{II}](L) - E[L/L^-](M^{III}) + \chi_i + \chi_o \quad (2)$$

$$h\nu = \Delta E[\text{Redox}] + \chi_i + \chi_o \quad (3)$$

where $\chi_i + \chi_o$ are respectively the inner (vibrational) and outer (solvent) reorganization energies, and $E[L/L^-](M^{III})$ signifies the reduction potential for ligand L bound to a M^{III} center. In practice only $E[L/L^-](M^{II})$ (the ligand reduction potential when it is attached to a central M^{II} ion) can be observed, where:

$$E[L/L^-](M^{III}) = E[L/L^-](M^{II}) + q \quad (4)$$

q is a positive number which effectively incorporates a collection of differential solvation energy terms, and a Coulombic term. We can then write:

$$\Delta E[\text{Redox}]' = E[L/L^-](M^{II}) - E[M^{III}/M^{II}](L) \quad (5)$$

$$h\nu = \Delta E[\text{Redox}]' - q + \chi_i + \chi_o \quad (6)$$

It is almost invariably true that $\Delta E[\text{Redox}]'$ under-estimates $h\nu$ such that the reorganization energy terms are larger than q.[4,61] The situation for **Band 5** is unusual in that

ΔE[Redox]' (couple I - couple II) over-estimates hν(**Band 5**) by some 1000 - 1500 cm^{-1} for all R, except R = NO_2, and R = OMe, where the agreement is exact. Thus, if the theory is formally applied, $q > \chi_i + \chi_o$. Since **Band 5** shows considerable charge transfer character, there is no compelling reason for believing that the reorganization energy is small. This would lead one to conclude that perhaps q is unusually large, consistent with 50:50 mixing of ligand and metal valence orbitals. Less mixing should lead to a smaller dependence of ligand reduction potential on the oxidation state of the metal.

c) Reorganization energy contributions - **Band 4**

A value for ΔE[Redox]', appropriate for **Band 4**, cannot be derived from electrochemistry since the loss of an electron from b_2 orbital, is not directly observed. Hence, a similar analysis to that performed on **Band 5** is not possible.

The small dependence of **Band 4** upon $\Sigma\sigma_p$ has indicated that this transition has little charge transfer character in keeping with the rR spectra reported above. However, there is an apparent pattern when these data are cross-correlated with bandwidths and ν(Ru-N) as shown in Figure 10. Since **Band 4** transitions are narrow, the errors on their energies are quite small.

The bandwidth measured at 1/e of the height of the band, $2\sigma^2$, is related to the displacements, Δ_k, and frequencies, ω_k, of the k^{th} vibrations coupled to the electronic transition via[62],

$$2\sigma^2 = \Sigma\, \Delta_k^2 \omega_k^2 \qquad (7)$$

where the parameter Δ_k is a dimensionless measure of the distortion[62] in the metal-ligand bond. Since the inner reorganization energy can be written as a sum over $K_q\Delta_k^2$, where K_q is the force constant of the bond, the bandwidth and reorganization energy are closely related.

A strictly parallel dependence of the b_2 and $2b_2^*$ energy levels upon the Hammett $\Sigma\sigma_p$ parameter would predict no dependence of the energy of **Band 4** upon $\Sigma\sigma_p$ except due to reorganization energy. Thus we may seek to attribute the pattern in Figure 10 to reorganization energy variations with substituent. The narrowness of **Band 4** reflects the fact that distortion

proceeds essentially along one coordinate (Ru-N) and that the frequency thereof is relatively small (approx. 600 cm^{-1}). Figure 10 shows that these parameters do behave in an overall parallel fashion with the energy of **Band 4**, confirming that the small variations with $\Sigma\sigma_p$ do reflect variations in reorganization energy.

The behaviour of **Band 4** in the R_2-bqdi species contrasts with that of the b_2 --> $2b_2^*$ transition in the less mixed R_2-sqdi species (**Band 9**) which, in its dependence upon $\Sigma\sigma_p$, is a more typical MLCT transition. However, the bandwidths of **Band 9** are comparable to those of **Band 4** and the parallelism that exists between the transition energy and bandwidth in the R_2-bqdi complexes also occurs in the R_2-sqdi complexes. Note that the R = NO_2 species has both unusually large bandwidth and transition energy which do not follow the general trend to lower energies with increasing $\Sigma\sigma_p$. This species has lower symmetry than the disubstituted species and it is possible that two transitions may lie under the band envelope.

Conclusions and Summary

If the mixing in the b_2 and $2b_2^*$ levels in these species is approaching 50:50, d(yz) + π^*(bqdi), then there is a significant formal Ru^{III}sqdi contribution to the Ru^{II}bqdi ground state, in agreement with the conclusion of Carugo et al.[40] In such a case there will be little substituent dependence of the b_2 ---> $2b_2^*$ transition energy, as is the case here, and the small variations which are observed (Figure 10) reflect variations in reorganization energy, χ_i, from one complex to another.

The apparent ambiguity between the description as Ru^{II}bqdi or Ru^{III}sqdi can now be rationalized in terms of the specific orbitals involved in the various electronic transitions, and the strong mixing. The a_1,$2a_2$ orbitals are mainly metal in character so that transitions therefrom, specifically **Band 3**, Ru a_1,$2a_2$ --> π^*(1) bpy, and **Band 5**, Ru a_1,$2a_2$ --> $2b_2^*$, appear strongly MLCT in character and have normal, i.e not especially narrow, bandwidths. With increasing electron acceptor character of the diimine ligand, electron density is drained off the metal centre and the a_1,$2a_2$ orbitals are stabilized. The direction of shift of the MLCT transitions is dictated by the dependence of the metal and terminal MO's on substituent, the

latter being assumed zero for $\pi^*(1)$ bpy, and being progressively stabilized with increasing acceptor ability for $2b_2^*$.

Band 4 (b_2 --> $2b_2^*$) involves a transition between levels which have roughly 50% metal and 50% ligand character so that it is not a charge transfer transition at all, but rather an internal transition of the total molecular complex; a situation discussed previously by Kaim.[63]. It may be called a metal-ligand to metal-ligand transition, MLML, to distinguish it from an internal transition of the ligand alone. It has characteristics similar to a σ --> σ^* transition in a metal-metal bonded species, L_nMML_n, such as being strongly localized in the molecule, having bonding to anti-bonding character, narrow bandwidth, and being absent from the spectra of the monomeric counterparts. Accordingly, we have also observed that photochemical excitation may cause metal-ligand dissociation in these species, but this has not yet been studied in detail.

Finally, the formal values for the E_L parameter[50] noted in Table II are approximate since couple I is not a pure Ru^{III}/Ru^{II} couple but contains a contribution from the ligand. The effect of "filtering out" the ligand contribution is likely to reduce the overall range of E_L values for this series of complexes.

Acknowledgements. We are indebted to the Natural Sciences and Engineering Research Council (Ottawa) and the Office of Naval Research (Washington) for financial support. We also thank Prof. William J. Pietro for access to, and guidance in using, the Spartan software, Prof. D. J. Stufkens and Dr. Th. L. Snoek for the resonance Raman data, Xiuyu Tai, and Lori Payne for technical support, and the Johnson-Matthey Company for the loan of ruthenium trichloride.

Bibliography

1. Kessel, S. L.; Emerson, R. M.; Debrunner, P. G.; Hendrickson, D. N.; Inorg. Chem. **1980**, 19, 1170.

2. Bhattacharya, S.; Pierpont, C. G. Inorg. Chem. **1991**, 30, 1511 and 2906; Bhattacharya, S.; Pierpont, C. G. Inorg. Chem. **1992**, 31, 35, and references therein.

3. Harmalker, S.; Jones, S. E.; Sawyer, D. T. Inorg. Chem. **1983**, 22, 2790.

4. Haga, M.-A.; Dodsworth, E. S.; Lever, A. B. P. Inorg. Chem. **1986**, 25, 447.

5. Stufkens D. J.; Snoeck Th. L.; Lever A. B. P. Inorg. Chem. **1988**, 27, 935.

6. Lever, A. B. P.; Auburn, P. R.; Dodsworth, E. S.; Haga, M.-A.; Liu, W.; Melnik, M.; Newin, W. A. J. Am. Chem. Soc. **1988**, 110, 8076.

7. Auburn, P. R.; Dodsworth, E. S; Haga, M.; Liu, W.; Nevin, W. A.; Lever, A. B. P. Inorg. Chem., **1991**, 31, 3502.

8. Stufkens, D. J.; Snoeck, Th. L.; Lever, A. B. P. Inorg. Chem. **1988**, 27, 953

9. Thompson, J. S.; Calabrese, J. C. Inorg. Chem. **1985**, 24, 3167.

10. Sofen, S. R.; Ware, D. C.; Cooper, S. R.; Raymond, K. N. Inorg. Chem. **1979**, 18, 234.

11. Boone, S. R.; Pierpont, C. G. Inorg. Chem. **1987**, 26, 1769.

12. Espinet P.; Bailey, P. M.; Maitlis, P. M. J. Chem. Soc., Dalton Trans. **1979**, 1542.

13. Pierpont, C. G.; Buchanan, R. M. Coord. Chem. Rev. **1981**, 38, 45.

14. Cooper, S. R.; Koh, Y. B.; Raymond, K. N. J. Am. Chem. Soc. **1982**, 102, 5092.

15. (a) Benelli, C.; Dei, A.; Gatteschi, D.; Pardi, L. Inorg. Chem. **1989**, 28, 1476; (b) Benelli, C.; Dei, A.; Gatteschi, D.; Güdel, H. U.; Pardi, L. Inorg. Chem. **1989**, 28, 3091; (c) Benelli, C.; Dei, A.; Gatteschi, D.; Pardi, L. Inorg. Chem. **1990**, 29, 3409.

16. Bruni, S.; Cariati, F.; Dei, A.; Gatteschi, D. Inorg. Chim. Acta, **1991**, 186, 157.

17. Dei, A.; Gatteschi, D.; Pardi, L.; Barra, A. L.; Brunel, L. C. Chem. Phys. Lett., **1990**, 175, 589; Dei, A.; Pardi, L. Inorg. Chim. Acta, **1991**, 181, 3.

18. Masui, H.; Lever, A. B. P.; Auburn, P. A. Inorg. Chem. **1991**, 30, 2402.

19. Auburn, P. R.; Lever, A. B. P. Inorg. Chem., **1990**, 29, 2551.

20. Balch, A. L.; Holm, R. H. J. Am Chem. Soc. **1966**, 88, 5201.

21. Baikie, P. E.; Mills, O. S. Inorg. Chim. Acta **1967**, 1, 55.

22. Duff, E. J. J. Chem. Soc. (A), **1968**, 434.

23. Warren, L. F. Inorg. Chem. **1977**, 16, 2814.

24. Reinhold, J.; Benedix, R.; Birner, P.; Hennig, H. Inorg. Chim. Acta **1979**, 33 209.

25. Vogler, A.; Kunkely, H. Angew. Chem., Int. Ed. Engl. **1980**, 19, 221.

26. Belser, P.; von Zelewsky, A.; Zehnder, M. Inorg. Chem. **1981**, 20, 3098.

27. El'Cov, A. V.; Maslennikova, T. A.; Kukuschkin, V. Ju.; Shavurov, V. V. J. Prakt. Chem. **1983**, B325, S27.

28. Pyle A. M. ; Barton, J. K. Inorg. Chem. **1987**, 26, 3820.

29. Pyle A. M. ; Chiang, M. Y. ; Barton, J. K. Inorg. Chem. **1990**, 29, 4487.

30. Thorn, D. L.; Hoffmann, R. Nouv. J. Chim. **1979**, 3, 39.

31. Peng, S.-M.; Chen, C.-T.; Liaw, D.-S.; Chen, C.-I.; Wang, Y. Inorg. Chim. Acta **1985**, 101, L31.

32. Christoph, G. G.; Goedken, V. L. J. Am. Chem. Soc. **1973**, 95, 3869.

33. Hall, G. S.; Soderberg, R. H. Inorg. Chem. **1968**, 7, 2300.

34. Gross, M. E.; Ibers, J. A.; Trogler, W. C. Organometallics **1982**, 1, 530.

35. Zehnder, M.; Loliger, H. Helv. Chim. Acta **1980**, 63, 754.

36. Danopoulos, A. A.; Wong, A. C. C.; Wilkinson, G.; Hursthouse, M. B.; Hussain, B. J. Chem. Soc., Dalton Trans. **1990**, 315.

37. Nemeth, S.; Simandi, L. I.; Argay, G.; Kalman, A. Inorg. Chim. Acta **1989**, 166, 31.

38. Joss, S.; Hasselbach, K. M.; Buergi, H. B.; Wordel, R.; Wagner, F. E.; Ludi, A. Inorg. Chem., **1989**, 28, 1815.

39. Rieder, K.; Hauser, U.; Sieganthaler, H.; Schmidt, E.; Ludi, A. Inorg. Chem., **1975**, 14, 1902.

40. Carugo, O.; Djinovic, K.; Rizzi, M.; Castellani, C. B. J. Chem. Soc. Dalton Trans. **1991**, 1551.

41. Magnuson, R. H.; Taube, H. J. Am. Chem. Soc. **1975**, 97, 5129.

42. Perrin, D. D.; Armarego, W. L. F. "Purification of Laboratory Chemicals", 3rd Edn; Pergamon Press plc. 1988

43. Gennett, T.; Milner, D. F.; Weaver, M. J. J. Phys. Chem. **1985**, 89, 2787.

44. Krejcik, M.; Danek, M.; Hartl, F., J. Electroanal. Chem., **1991**, 317, 179.

45. Stufkens, D. J.; Snoeck, Th. L.; Dodsworth, E. S.; Masui, H.; Metcalfe, R. A.; Lever, A. B. P. to be submitted for publication.

46. Nakamura, M.; Toda, M.; Saito, H.; Ohkura, Y. Anal. Chim. Acta. **1982**, 134, 39.

47. Ehrlich, J.; Bogert, M. T. J. Org. Chem. **1947**, 12, 522.

48. Sullivan, B. P.; Salmon, D. J.; Meyer, T. J. Inorg. Chem. **1978**, 17, 3334.

49. Hansch, C.; Leo, A.; Taft, R. W. Chem. Reviews, **1991**, 91, 165.

50. Lever, A. B. P. Inorg. Chem. **1990**, 29, 1271.

51. Masui, H.; Lever, A. B. P. to be submitted for publication.

52. Dodsworth E. S.; Lever A. B. P. Chem. Phys. Lett. **1986**, 124, 152.

53. Mallick, P. K.; Danzer, G. D.; Strommen, D. P.; Kincaid, J. R. J. Phys. Chem. **1988**, 92, 5628.

54. Reimers, J. R.; Hush, N. S. Inorg. Chem. **1990**, 29, 3686.

55. (a) Gutmann, V. Electrochim. Acta. **1976**, 21, 661.

(b) Hampe, M. J. Ger. Chem. Eng. **1986**, 9, 251.

56. A plot of $\log\{(A_f - A)/(A - A_i)\}$ versus E_{app} (for $[Ru(bpy)_2(Cl_2\text{-bqdi})]^{2+}$ in acetonitrile), yields a linear correlation with a slope of 20.0 ($\sigma = \pm 0.4$) V^{-1}, a value of 16.95 V-1 being expected for a reversible one electron transfer process. Here, A is the peak absorbance of **Band 4** at the various applied potentials, E_{app}, and A_i and A_f are the limiting absorbances before and after reduction respectively. The intercept yields an $E_{1/2}$ of -0.23 V compared with -0.28 V in Table II.

57. Balk, R. W.; Stufkens, D. J.; Crutchley, R. J.; Lever, A. B. P. Inorg. Chim. Acta **1982**, 64, L49.

58. Vlcek, A. A. Electrochim. Acta, **1968**, 13, 1063.

59. de la Rosa, R.; Chang, P. J.; Salaymeh, F.; Curtis, J. C. Inorg. Chem. **1985**, 24, 4229.

60. Mines, G. A; Roberts, J. A.; Hupp, J. T. Inorg. Chem **1992**, 31, 125.

61. Ghosh, P.; Chakravorty, A. Inorg. Chem. **1984**, 23, 2242.

62. Tutt, L.; Zink, J. I. J. Am. Chem. Soc. **1986**, 108, 5830.

63. Kaim, W.; Gross, R. Comments Inorg. Chem. **1988**, 7, 269.

Table I. Ab Initio Orbital Energy Calculations of R_2-bqdi ligands.

Species	LUMO(π^*)	HOMO(π)	SHOMO[a,b]	THOMO[a](σ)
4-NO_2	0.11331	-0.27167	-0.34942	-0.36180
4,5-Cl_2	0.11639	-0.26704	-0.35872	-0.36014
H	0.14884	-0.24404	-0.33413	-0.35810
4,5-Me_2	0.15332	-0.23167	-0.32769	-0.34466
4,5-$(OMe)_2$	0.15535	-0.22219	-0.29270	-0.32730
4,5-$(NH_2)_2$	0.17337	-0.19961	-0.26023	-0.31138

Energies are in Hartrees. 1 Hartree = 219489 cm^{-1}. a) Second (SHOMO) and third (THOMO) highest occupied molecular orbitals. b) Orbital is of σ symmetry for R = NO_2, H, Me and π for R = Cl, OMe and NH_2.

Table II. Redox potentials of $[Ru(bpy)_2(R_2\text{-bqdi})]^{2+}$ Complexes[a].

Species	Ru^{III}/Ru^{II} I	bqdi/sqdi II	sqdi/opda III	bpy/bpy$^-$(1) IV	bpy/bpy$^-$(2) V	EL[b]	$\Sigma\sigma_p$
4,5-$(NH_3^+)_2$							1.20
4-NO_2[c]	1.57	0.08	-0.69	-1.62	-1.86	0.38	0.78
4,5-Cl_2	1.50[d]	-0.28	-0.96	-1.75	-2.19[e]	0.33	0.45
H	1.37	-0.45	-1.13[e]	-1.70[d]	-1.94[d]	0.28	0.00
4,5-$(NH_2)(NH_3^+)$							-0.06
4,5-Me_2	1.32	-0.56	-1.21	-1.77	-1.94[d]	0.25	-0.34
4,5-$(OMe)_2$	1.15	-0.73	-1.26	-1.74[e]	-1.86[e]	0.16	-0.54
4,5-$(NH_2)_2$	0.83	-0.94[d,f]	-1.43[e]	-1.78[e]	-2.01[d,f]	0.01	-1.32

a) Obtained in 0.1 M $TBAPF_6$ solutions in acetonitrile; potentials in V vs SCE. b) See text for comments on these values; also see ref.[48]. c) Mono-substituted at 4 position. d) Irreversible. e) Quasi-reversible. f) Peak potential.

Table III. Electronic Spectra of Complexes[a] (cm^{-1})

$[Ru(bpy)_2(R_2\text{-bqdi})]^{2+}$ Complexes	$\pi \rightarrow \pi^*$ o-phenylene	Ru d $\rightarrow \pi^*$(1) bpy	$b_2 \rightarrow 2b_2^*$	Ru $a_1,2a_2 \rightarrow 2b_2^*$
Species	**Band 1**	**Band 3**	**Band 4**	**Band 5**
4,5-$(NH_3^+)_2$[b]		25670(3.73)	19700(4.32)(Δ3200)[c]	11050(2.36)(Δ6500)
4-NO_2[d]	35840(4.57)	24040[e](3.90)	18980(4.31)(Δ2850)	11750(2.49)(Δ4300)
4,5-Cl_2	35720(4.62)	23760(3.75)	19030(4.40)(Δ2750)	12640(2.07)(Δ3700)
H_2	35650(4.56)	22810(3.84)	19440(4.30)(Δ2850)	13300(2.74)
H2[f]	35540	22730	19490 (Δ2750)	13290
4,5-$(NH_2)(NH_3^+)$[g]		22620(3.85)	18800(4.43)(Δ3050)	13750(2.66)(Δ5600)
4,5-$(CH_3)_2$	35470	22230(3.90)	19180(4.40)(Δ2600)	13700(2.33)(Δ3900)
4,5-$(OCH_3)_2$	35100	22910(3.85)	18850(4.49)(Δ2200)	15000(2.40)(Δ4800)
4,5-$(NH_2)_2$[h]	34620	21100(4.04)	18120(4.57)(Δ1850)	15600sh

$[Ru(bpy)_2(R_2\text{-sqdi})]^+$ Complexes[i]	Ru d $\rightarrow \pi^*$(2) bpy	Ru d $\rightarrow \pi^*$(1) bpy	$b_2 \rightarrow 2b_2^*$	Ru $a_1,2a_2 \rightarrow 2b_2^*$
Species	**Band 7**	**Band 8**	**Band 9**	**Band 10**
4-NO_2[d]	33000sh	21960(4.07) 24200sh	15400(4.24)(Δ2600)[c]	12370
4,5-Cl_2	31150sh	21000(4.07)	15350(4.16)(Δ1650)	12300
H_2	29070(3.91)	23200(3.88) 22100sh 20100 19400sh	16000(4.05)(Δ2050)	11100
4,5-$(CH_3)_2$	28500(3.93)	22500sh 21900(3.93) 19850(4.02) 19100sh	16150(4.02)(Δ2300)	und.
4,5-$(OCH_3)_2$[j]	29600	21980 21000 28000sh	16250 (Δ3000) 19490 19080sh	und.

Table III cont

$[Ru(bpy)_2(R_2\text{-opdaH}_2)]^{2+}$ Complexes[k]	π---> π^* o-phenylene	Ru d ---> π^*(2) bpy	Ru d ---> π^*(1) bpy
Species	**Band 11**	**Band 12**	**Band 13**
4-NO_2[d,l]	34370	30090	21790sh, 20840
4,5-Cl_2	34500	32400sh	21200
H_2	34350(4.40)	30000sh(3.62)	20900(3.73)
H_2[f]	und.	und.	20530
4,5-$(CH_3)_2$	35000 est	29650	20750
4,5-$(OCH_3)_2$	34450	32000sh	20750
4,5-$(NH_2)_2$	34500	31600	20550

$Ru(bpy)_2(R_2\text{-opda})$ Complexes[i]	Ru d ---> π^*(2) bpy	Ru d ---> π^*(1) bpy	$opda^{2-}$ ---> π^*(1) bpy LLCT
Species	**Band 15**	**Band 16**	**Band 17**
4-NO_2[d]	27320	18890	13980, 13000[m]
4,5-Cl_2	26820[j]	18490[j]	
4,5-Me_2	28100[j]	18700[j]	

a) Spectra were obtained in acetonitrile except where otherwise stated. Log(ϵ) in parenthesis. For **Band** numbering, see Figures. und. - undetermined. **Band 5** corresponds roughly with the difference in potential between couples I and II (Table 2) (see text); these values are 4-NO_2, 11750; 4,5-Cl_2, 14150; H, 14700; 4,5-$(CH_3)_2$, 15100; 4,5-$(OCH_3)_2$, 15100; 4,5-$(NH_2)_2$, 14150 cm^{-1}. b) Dissolved in concentrated H_2SO_4. c) Bandwidths at 1/e of height, in parentheses. d) Mono-substituted at 4 position. e) Identified in spectrum recorded at 77 K; at room temperature this absorption is obscured by a nitro related transition at 25,600 cm^{-1}. f) Dissolved in water. g) Dissolved in dilute 3 M HCl(aq). h) **Band 2** Ru d ---> π^*(2) bpy, may be identified in this complex at 30120(4.11) cm^{-1} i) Spectra

obtained in acetonitrile containing 0.3 M TBAP by controlled potential reduction of the bqdi species (see text). Where sqdi (or opdaH_2) spectra are not reported for a specific species, this is generally due to the instability of the reduced species. j) Isosbestics were lost halfway through electrolysis. Data were obtained from the last spectrum before loss of isosbestics. k) Except where indicated, obtained by dissolving the isolated complex in acetonitrile. l) Obtained in 5% HOAc in acetonitrile by Zn/Hg reduction of the NO_2-bqdi species. m) Tentative assigment.

Table IV. Solvatochromism of $[Ru(bpy)_2(R_2\text{-bqdi})]^{2+}$, R = Cl, NH_2 (cm^{-1}).

$[Ru(bpy)_2(R\text{-bqdi})]^{2+}$					R = Cl	R = NH_2
Solvent	DN[a]	Band 3[b]	Band 4[c]	Band 5[d]	Band 4[c]	Band 5[d]
CH_2Cl_2	0.0	--	--	--	21900	18200(1820)
DCE	0.0	--	--	--	21800	18100(1800)
MeCN	14.1	23750	19050(2750)	12750	21250	18200(1810)
PC	15.1	23650	19000(2600)	12700	21350	18000(1820)
Me_2CO	17.0	23550	19000(2720)	12200	21300	18100(1820)
EtOAc	17.1	23500	19050(2800)	13450	21100	18200(1740)
H_2O	18.0	23650	19050(2740)	12450	21350	18200(3580)
MeOH	19.0	23400	19050(2670)	12550	21150	18200(1910)
EtOH	20.0	23200	18950(2550)	12900	21150	18150(1830)
THF	20.0	23450	19000(2720)	12300	20950	18050(1880)
DMF	26.6	23000	18850(2860)	12950	20900	18000(1860)
DMA	27.8	23000	18900(2820)	12800	--	--
DMSO	29.8	22860	18850(2670)	12300	20900	17900(1930)
EtCOMe	--	23550	19000(2690)	12850	20900	17950(1840)
n-BuOH	--	22500	19000(2810)--	--	--	
n-PrOH	--	23150	19000(2690)	12650	--	--
HOAc	--	--	--	--	21400	18150(2200)

Abbreviations are those commonly used; note PC = propylene carbonate, DCE = 1,2-dichloroethane a) Donor number.[54] b) Ru $a_1,2a_2$ ---> $\pi^*(1)$ bpy. Values in parenthesis are halfbandwidths at 1/e of peak height. c) b_2 --> $2b_2^*$. d) Ru $a_1,2a_2$ ---> $2b_2^*$

Table V Regression Analysis for Data Shown in Figure 9

MO/couple	Slope(Std. Dev) (cm^{-1})	Const.(Std. Dev) (cm^{-1})	No. of points	Regression Coefficient
a_2	-3830(70)	-22400(110)	6	0.99
b_2	-3970(240)	-6000(500)	8	0.99
a_1,$2a_2$	-1630(210)	-350(440)	8	0.95
$2b_2^*$	-3500(170)	13000(360)	8	0.99
Couple I[a]	2840(290)	10900(490)	6	0.98
Couple II[a]	3730(460)	-3300(770)	6	0.97

a) Redox potentials converted to wavenumber, 1 eV = 8065 cm^{-1}.

Figure 1. Simplified molecular orbital model of the R_2-bqdi and R_2-sqdi complexes. The transition labels correspond to the band labels of Figure 4.

Figure 2. Cyclic voltammogram of $[Ru(bpy)_2(bqdi)]^{2+}$ complex in dry acetonitrile containing 0.1M $TBAPF_6$; potentials referenced to SCE.

Figure 3. The substituent dependence of the redox potentials of the R_2-bqdi complexes (V vs SCE). The equations of the lines are as follows (values in parentheses are standard deviations and R = regression coefficient):

(I) Ru^{III}/Ru^{II}: $E_{1/2} = 0.36(\pm0.035)\Sigma\sigma_p + 1.35(\pm0.024)$; R = 0.982.

(II) R_2-bqdi/R_2-sqdi: $E_{1/2} = 0.47(\pm0.065)\Sigma\sigma_p - 0.40(\pm0.045)$; R = 0.964.

(III): R_2-sqdi/R_2-opda: $E_{1/2} = 0.33(\pm0.053)\Sigma\sigma_p - 1.06(\pm0.037)$; R = 0.952.

(IV): bpy/bpy^-: $E_{1/2} = 0.059(\pm0.027)\Sigma\sigma_p - 1.72(\pm0.019)$; R = 0.733

Figure 4. Typical spectra of the orthophenylene complexes in the three redox forms. (···) $[Ru(bpy)_2(opdaH_2)]^{2+}$; (---) $[Ru(bpy)_2(sqdi)]^{+}$; (---) $[Ru(bpy)_2(bqdi)]^{2+}$. The data were obtained in acetonitrile. See Table III for assignments of identified transitions. **Band 2** was only clearly identified in the $Ru(bpy)_2(NH_2)_2$-bqdi species spectrum.

Figure 5. Resonance Raman spectra of the R_2-bqdi and R_2-sqdi complexes in CH_2Cl_2. a) $[Ru(bpy)_2(Cl_2\text{-bqdi})]^{2+}$, excited at 543nm. b) $[Ru(bpy)_2(Cl_2\text{-sqdi})]^{+}$, excited at 515nm. N.b. the fairly prominent peak at 600 cm^{-1} is due to excitation of a small quantity of unreduced bqdi species. c) $[Ru(bpy)_2(Cl_2\text{-sqdi})]^{+}$, excited at 620nm. Asterisks denote solvent Raman lines.

Figure 6. The substituent dependence of the various charge transfer bands of the R_2-bqdi complexes. The data were mainly obtained in acetonitrile except for the 4,5-NH_2,NH_3^+ and 4,5-$(NH_3^+)_2$ species, which were obtained in 3M HCl and concentrated H_2SO_4, respectively.

Figure 7. Titration of $[Ru(bpy)_2((NH_2)_2\text{-bqdi})]^{2+}$ in water with concentrated HCl, and following the intensity of **Band 3** (corrected for dilution). A datum collected in 25% sulfuric acid (pKa ~ -.95) wherein the species is believed to be diprotonated, yielded a value of .70 au in this figure.

Figure 8. A plot of the Ru --> $\pi^*(1)$ bpy transition energies as a function of Hammett $\Sigma\sigma_p$ for each redox form of the orthophenylene complexes. For the R_2-sqdi plot, the lower energy Ru a_1,a_2 --> $\pi^*(1)$ bpy band maximum was used where splitting of these transitions was observed.

Figure 9. A plot of the trends in molecular orbital energies of the R_2-bqdi complexes as a function of $\Sigma\sigma_p$ (see text). The energies are referenced to a fixed $\pi^*(1)$ bpy orbital and the a_1,$2a_2$ orbitals of the R = H species have been arbitrarily set to zero. The square symbols represent experimentally obtained redox potentials as described in the text.

Figure 10. Plots of a) the energy of **Band 4**, b) the bandwidth of **Band 4**, and c) the ν(Ru-N) FTIR data as a function of Hammett $\Sigma\sigma_p$ for the R_2-bqdi species. Electronic spectral were obtained from acetonitrile solutions while FTIR data were obtained from KBr pellets.

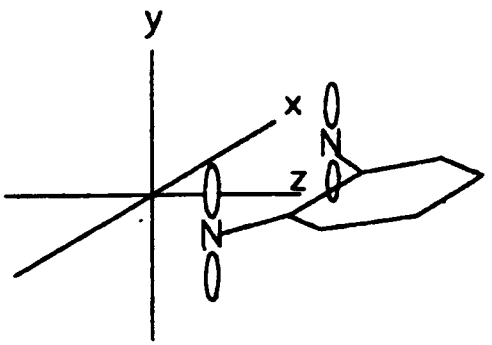
y
x
z
N
N

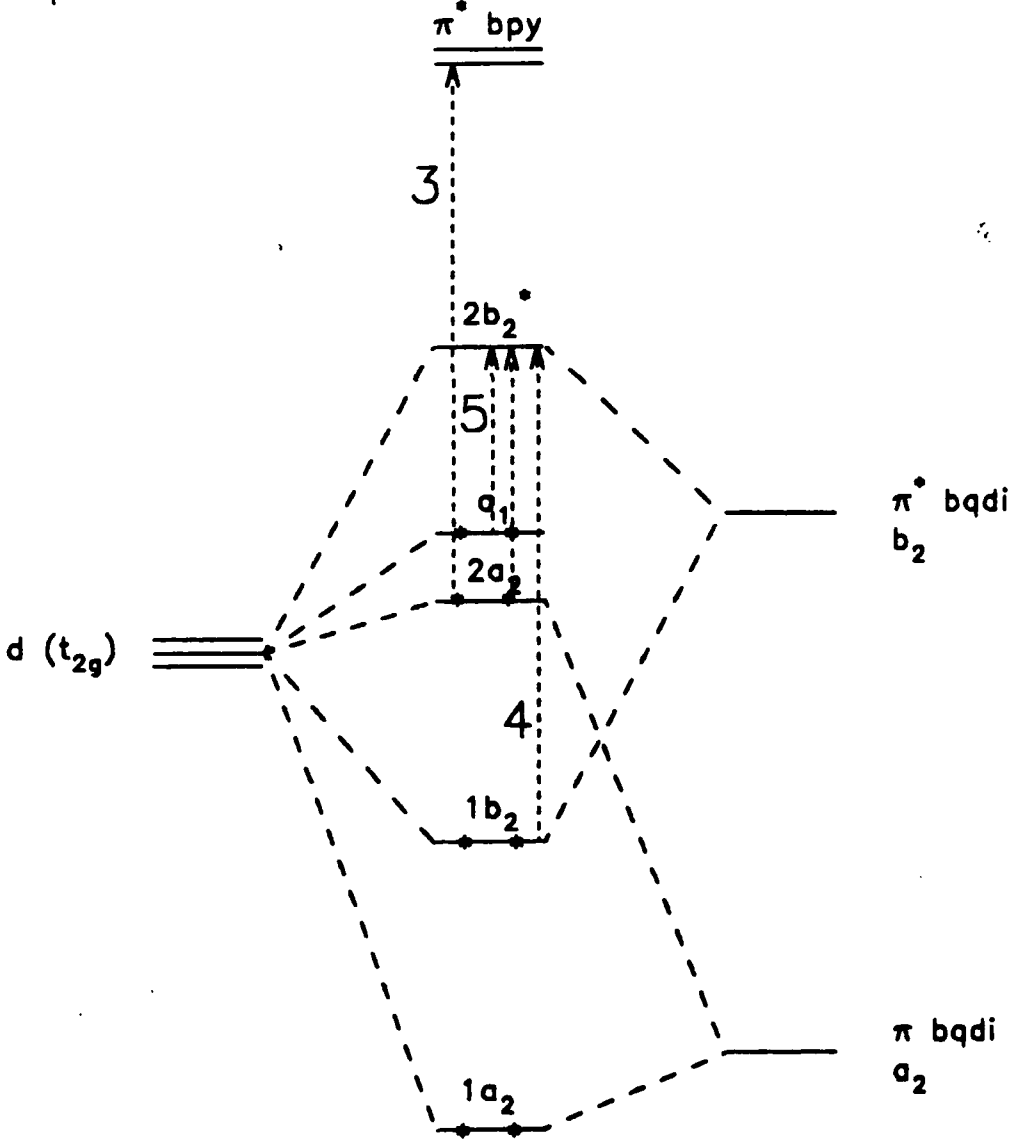
π* bpy
3
2b2*
5
q1
2a2
π* bqdi
b2
d (t2g)
4
1b2
π bqdi
a2
1a2

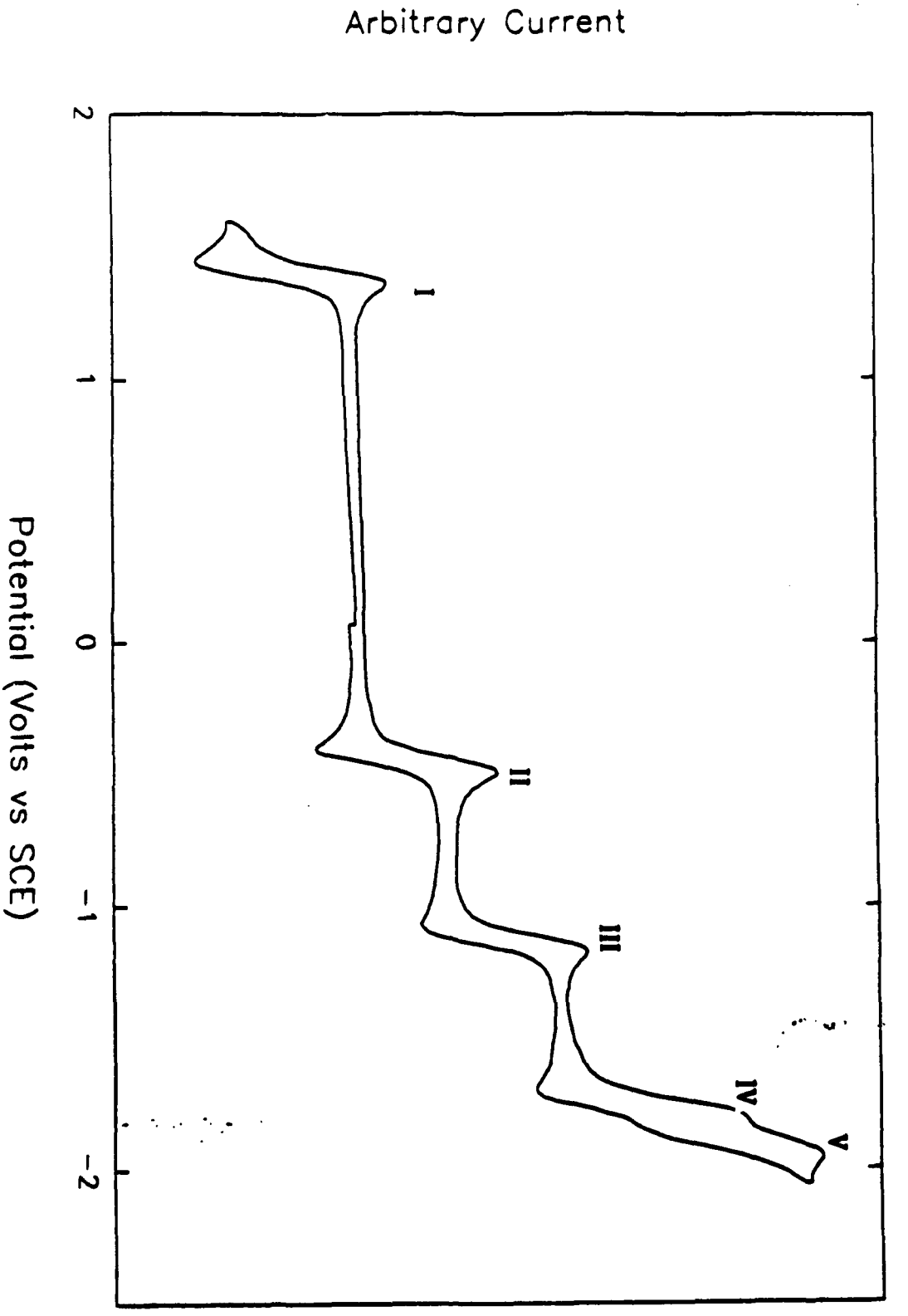
Arbitrary Current
Potential (Volts vs SCE)
2
1
0
-1
-2
I
II
III
IV
V

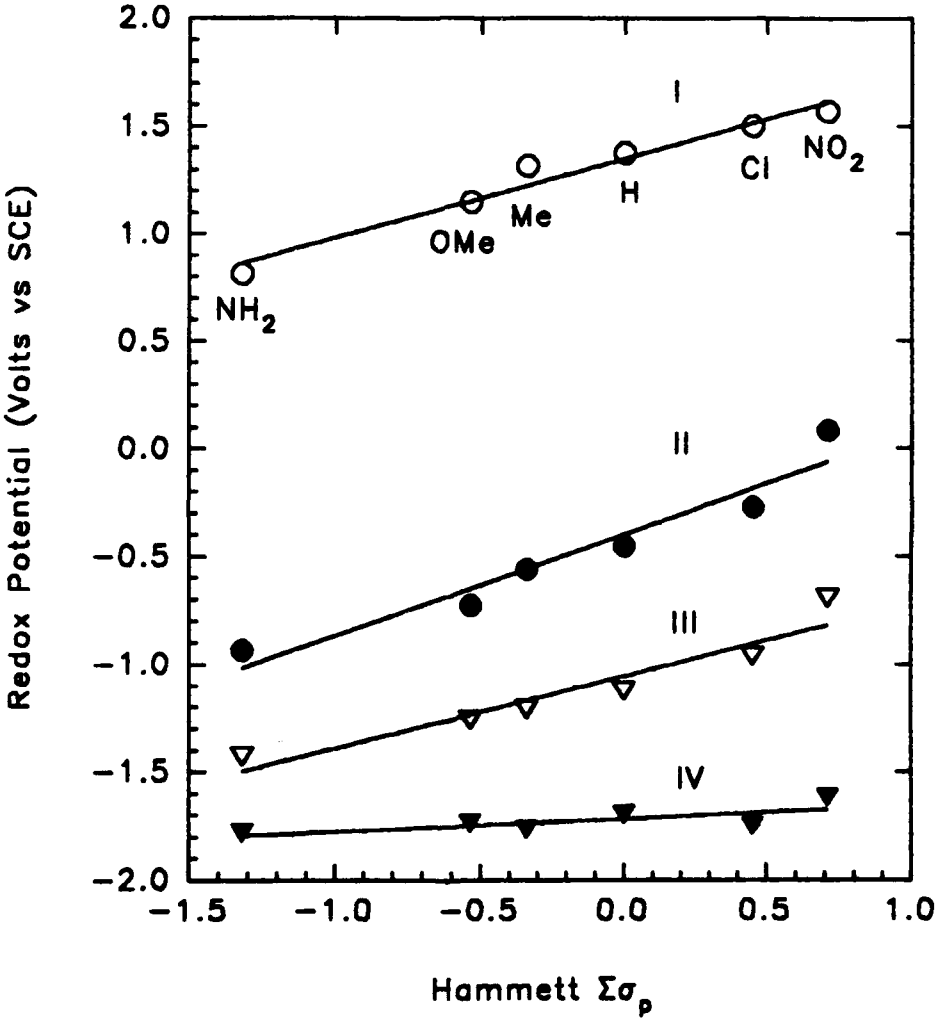
2.0
1.5
1.0
0.5
0.0
−0.5
−1.0
−1.5
−2.0
−1.5
−1.0
−0.5
0.0
0.5
1.0
Redox Potential (Volts vs SCE)
Hammett Σσp
I
II
III
IV
NH2
OMe
Me
H
Cl
NO2

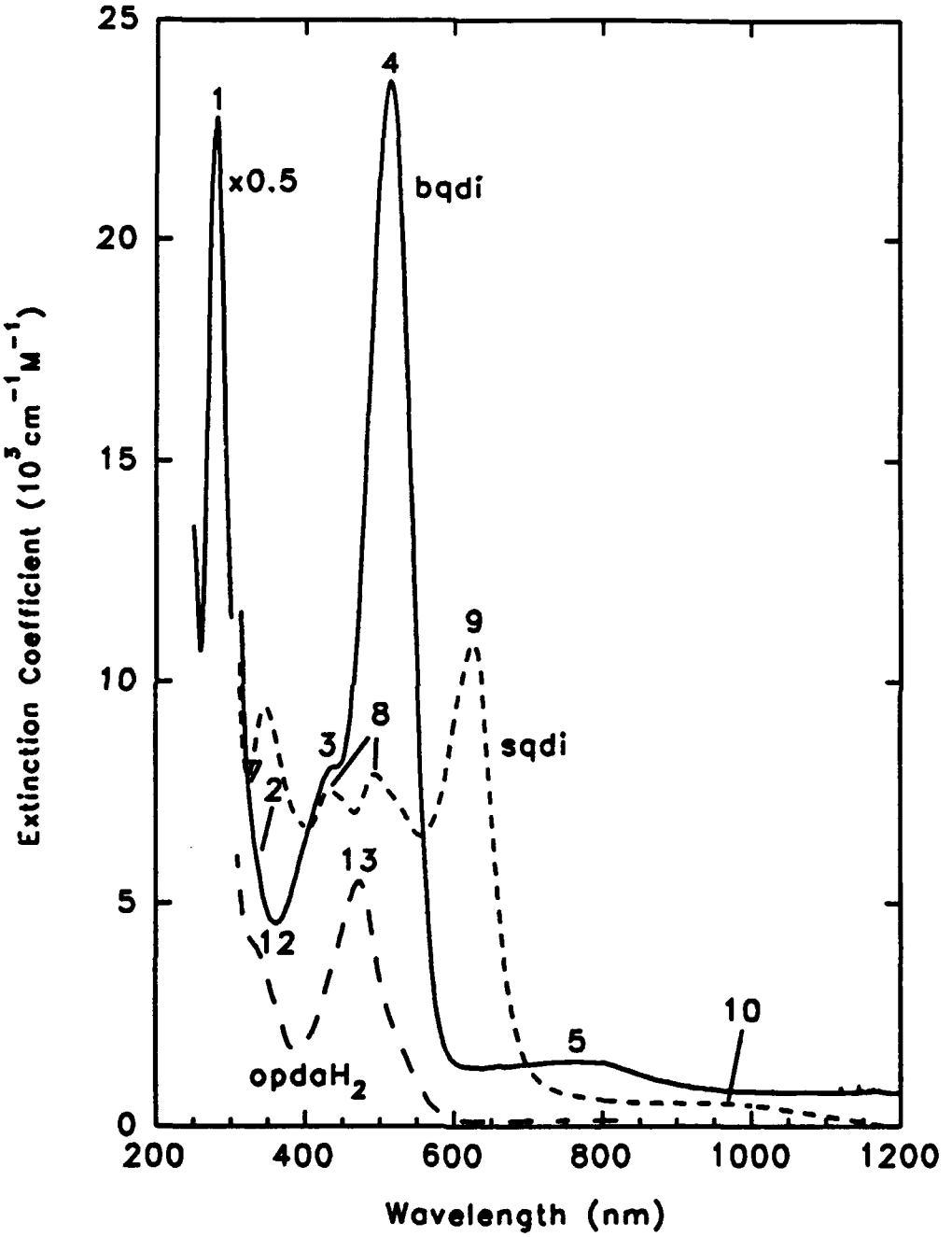
25
20
15
10
5
0
200
400
600
800
1000
1200
Extinction Coefficient ($10^3 cm^{-1} M^{-1}$)
Wavelength (nm)
1
x0.5
4
bqdi
9
sqdi
8
3
2
13
12
10
5
opdaH$_2$

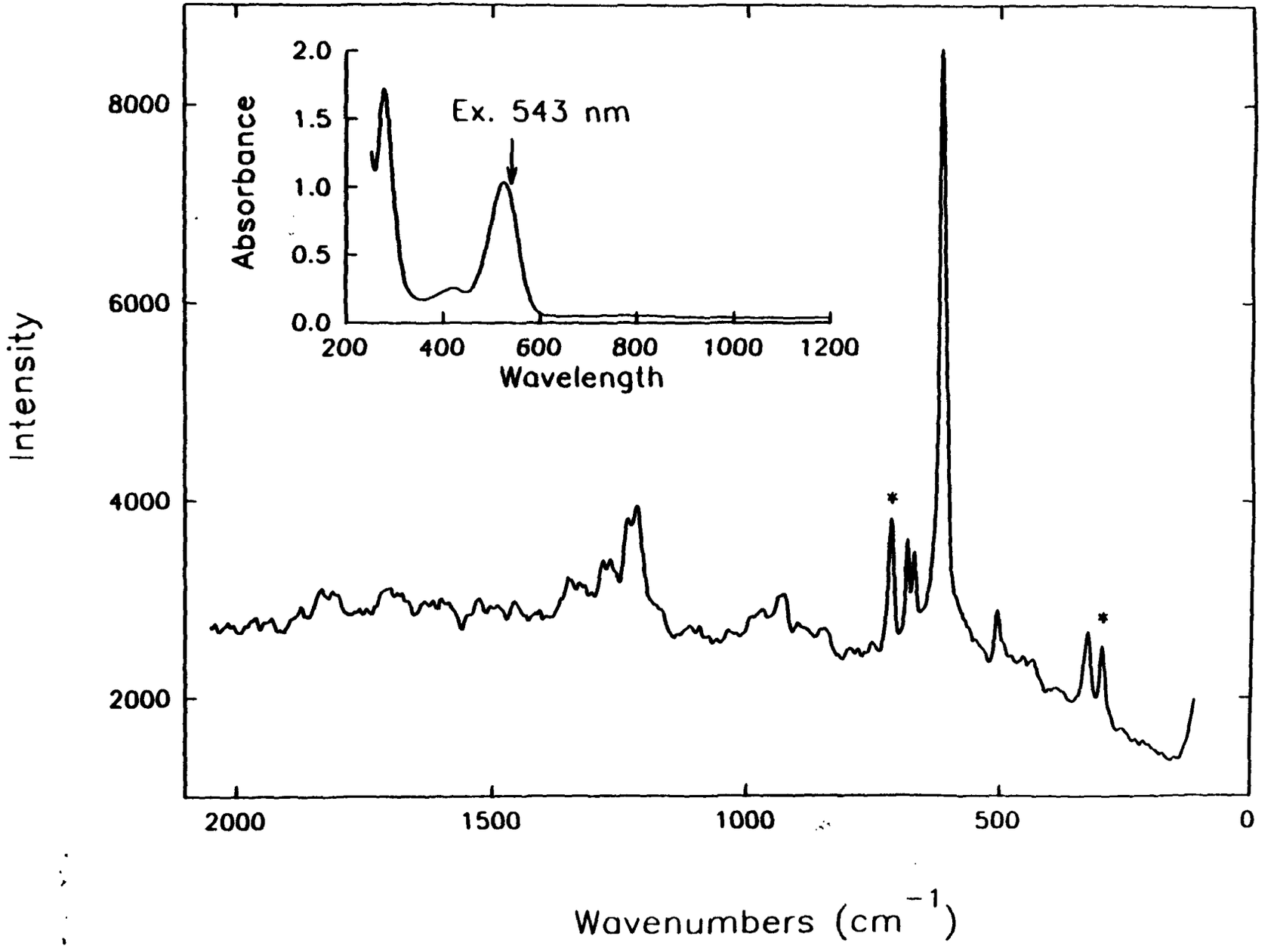
Intensity
8000
6000
4000
2000
2000
1500
1000
500
0
Wavenumbers (cm^{-1})
*
*
Absorbance
2.0
1.5
1.0
0.5
0.0
Ex. 543 nm
200
400
600
800
1000
1200
Wavelength

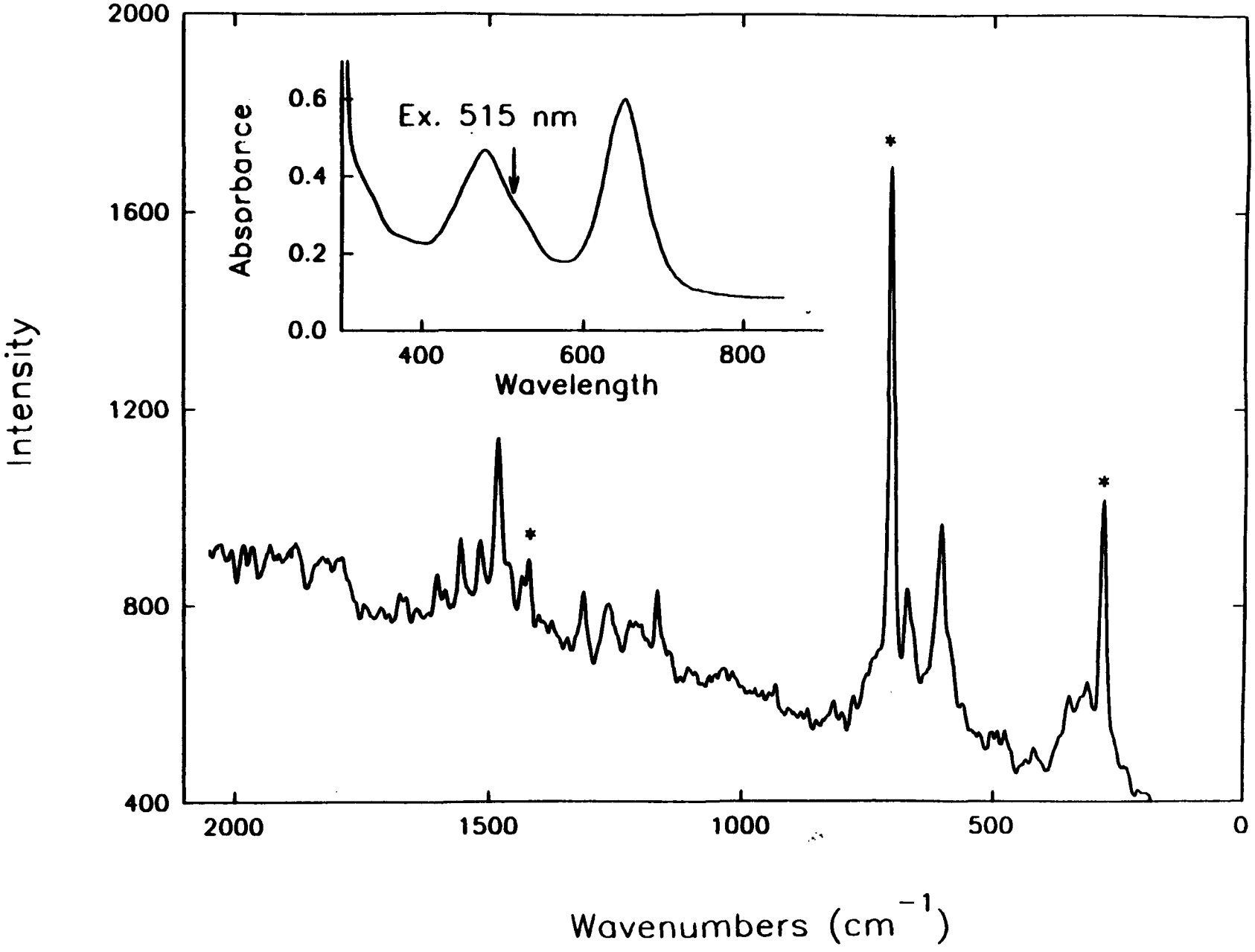
Intensity
2000
1600
1200
800
400
2000
1500
1000
500
0
Wavenumbers (cm^{-1})
*
*
*
Absorbance
0.6
0.4
0.2
0.0
Ex. 515 nm
400
600
800
Wavelength

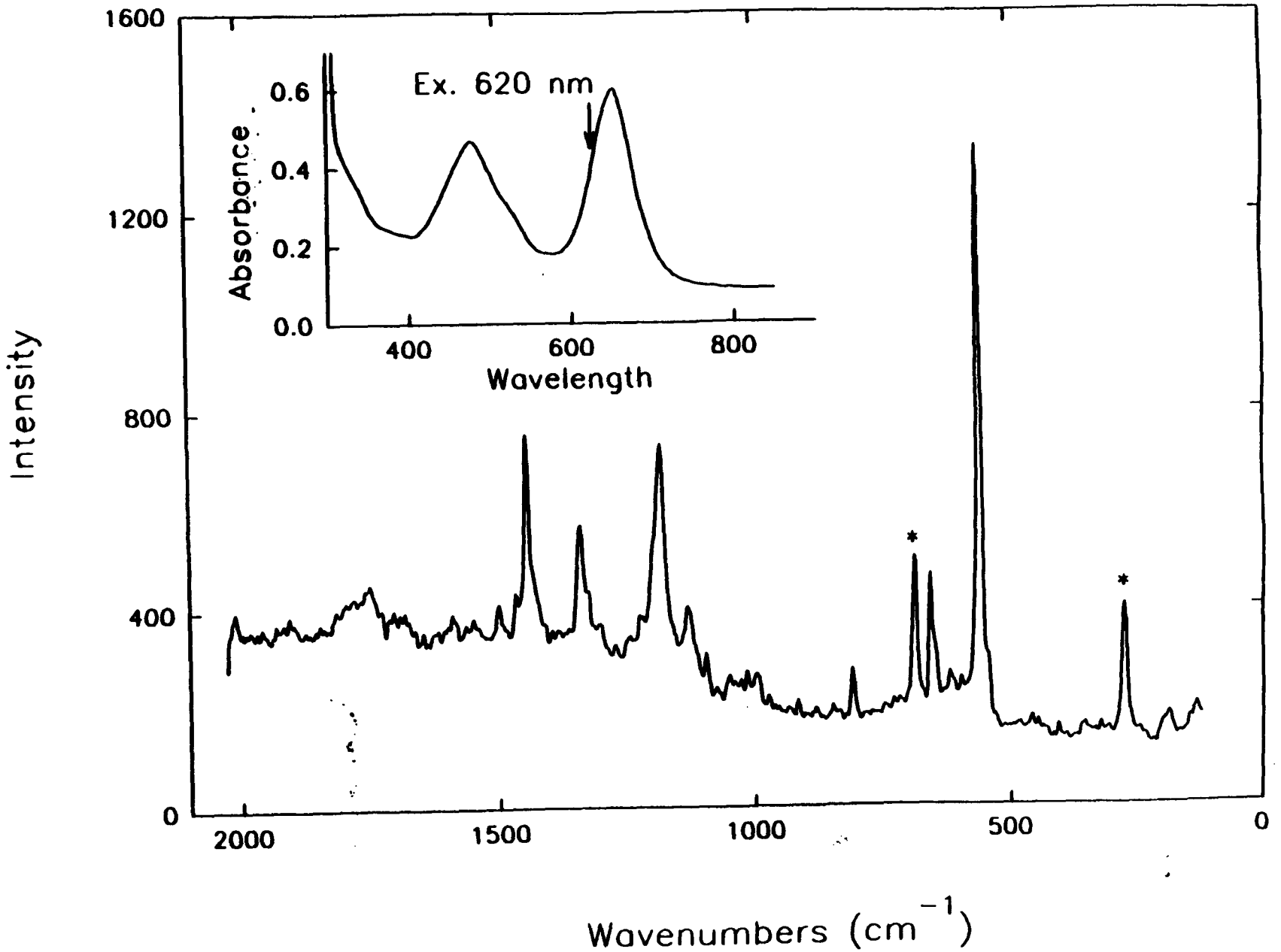
Ex. 620 nm
Absorbance
0.6
0.4
0.2
0.0
400
600
800
Wavelength
1600
1200
800
400
0
Intensity
2000
1500
1000
500
0
Wavenumbers (cm^{-1})
*
*

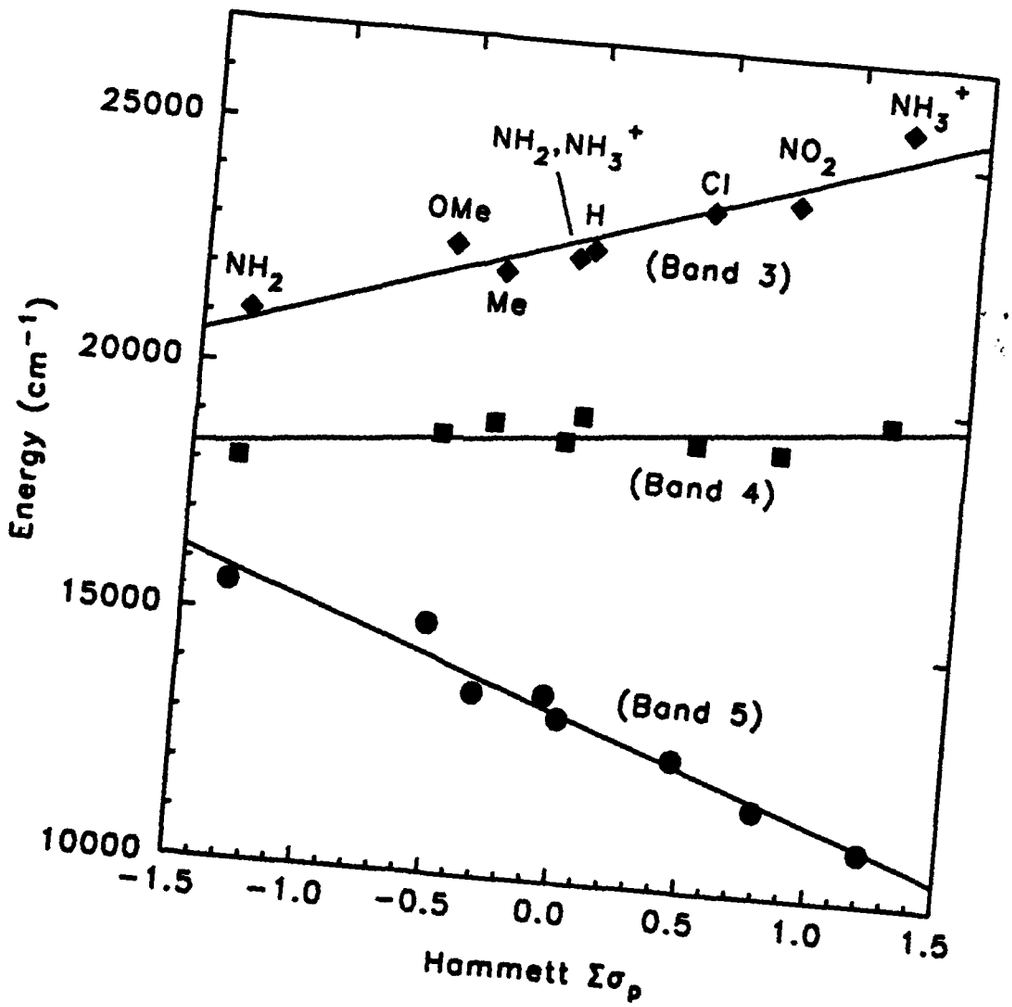
25000
20000
15000
10000
Energy (cm⁻¹)
NH2
OMe
Me
H
NH2,NH3+
Cl
NO2
NH3+
(Band 3)
(Band 4)
(Band 5)
-1.5
-1.0
-0.5
0.0
0.5
1.0
1.5
Hammett Σσp

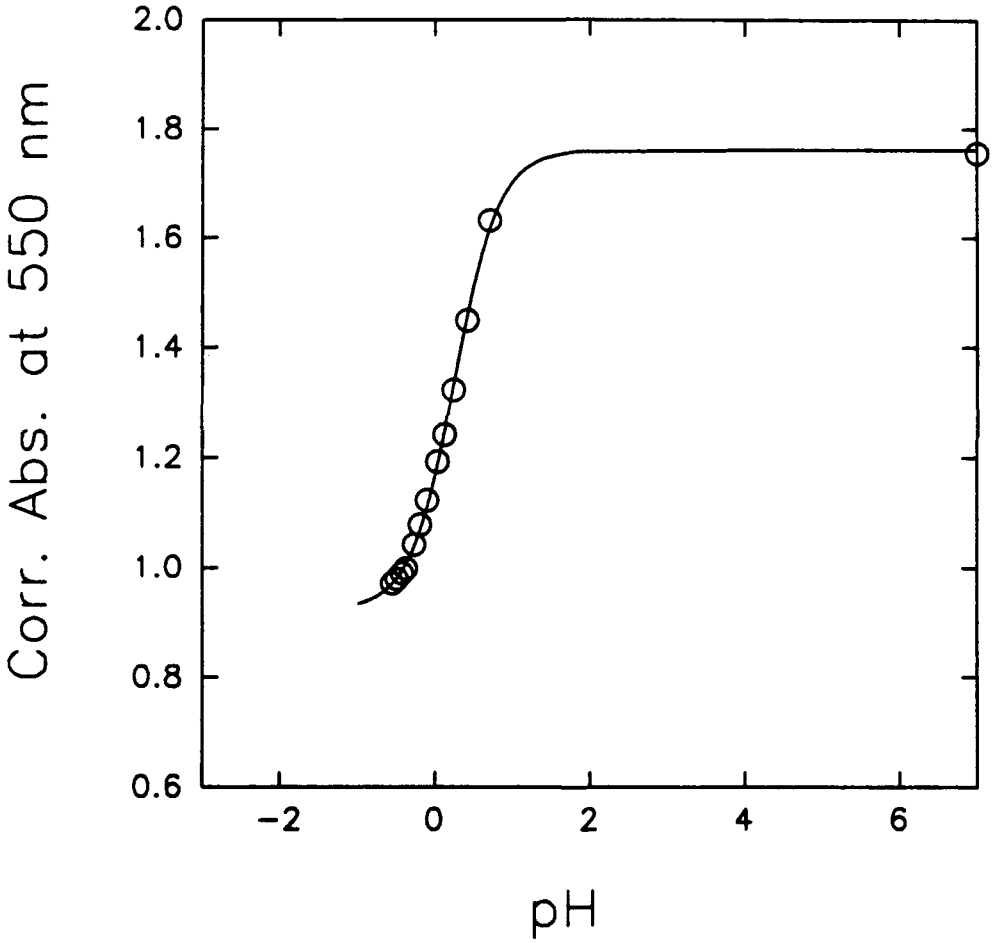
Corr. Abs. at 550 nm
2.0
1.8
1.6
1.4
1.2
1.0
0.8
0.6
−2
0
2
4
6
pH

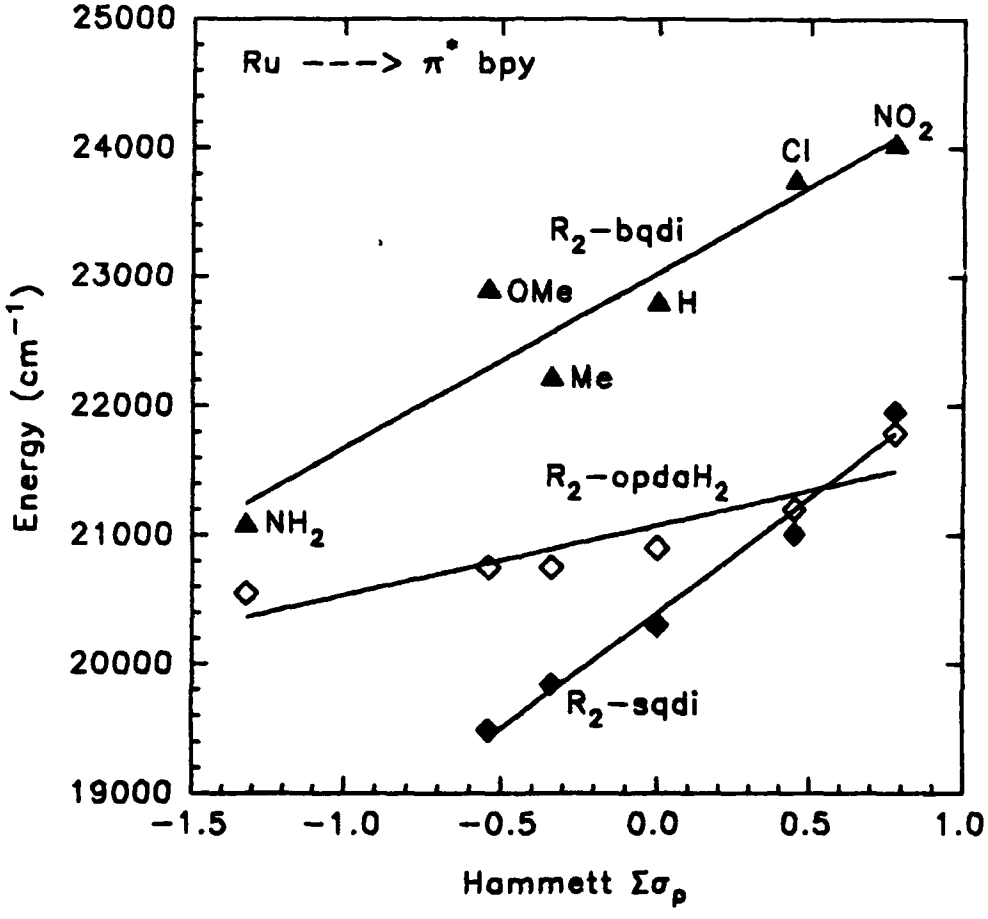
Ru ---> π* bpy
NO2
Cl
R2–bqdi
OMe
H
Me
R2–opdaH2
NH2
R2–sqdi
Energy (cm-1)
25000
24000
23000
22000
21000
20000
19000
−1.5
−1.0
−0.5
0.0
0.5
1.0
Hammett Σσp

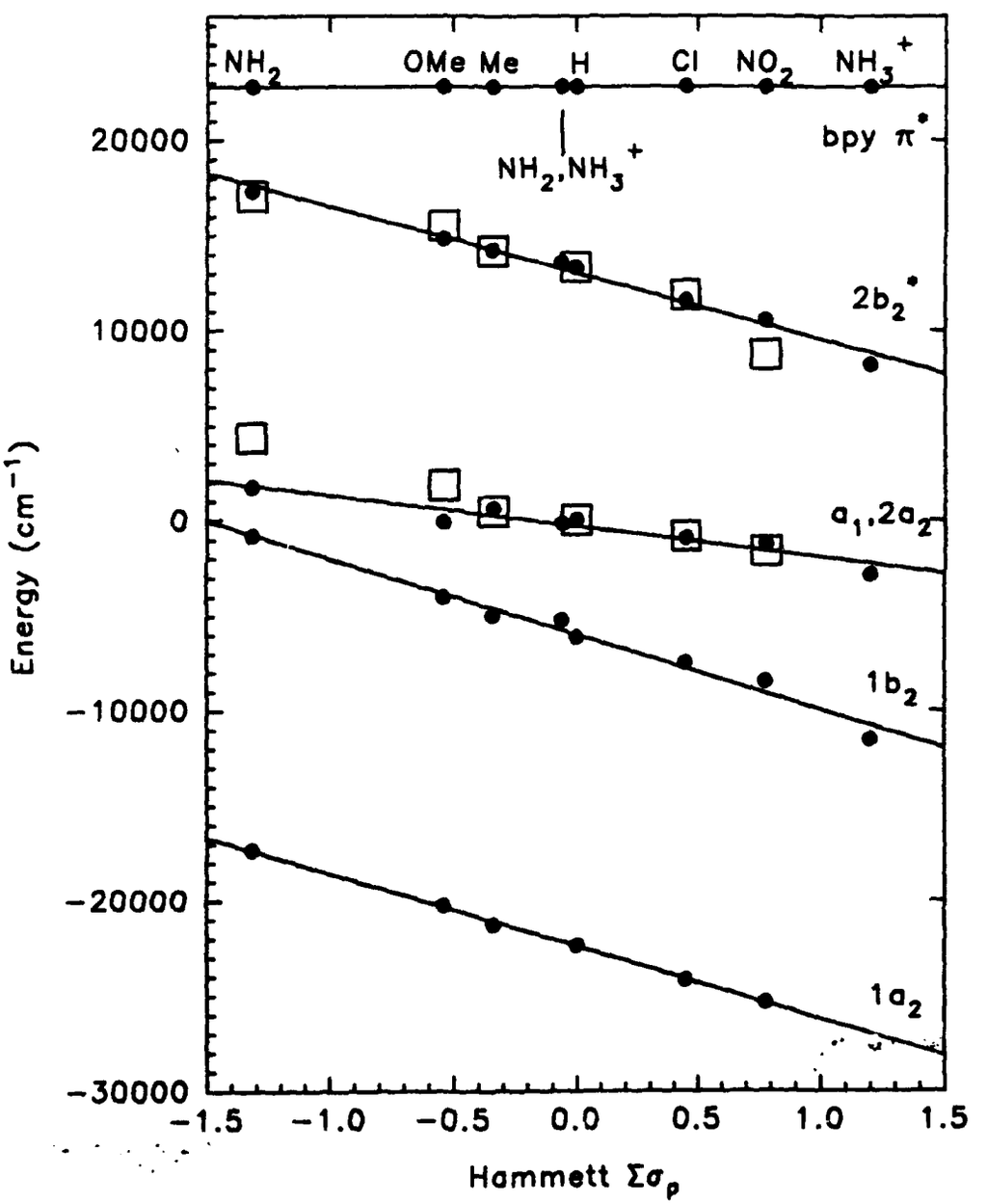
NH2
OMe
Me
H
Cl
NO2
NH3+
NH2,NH3+
bpy π*
2b2*
a1,2a2
1b2
1a2
20000
10000
0
−10000
−20000
−30000
−1.5
−1.0
−0.5
0.0
0.5
1.0
1.5
Energy (cm−1)
Hammett Σσp

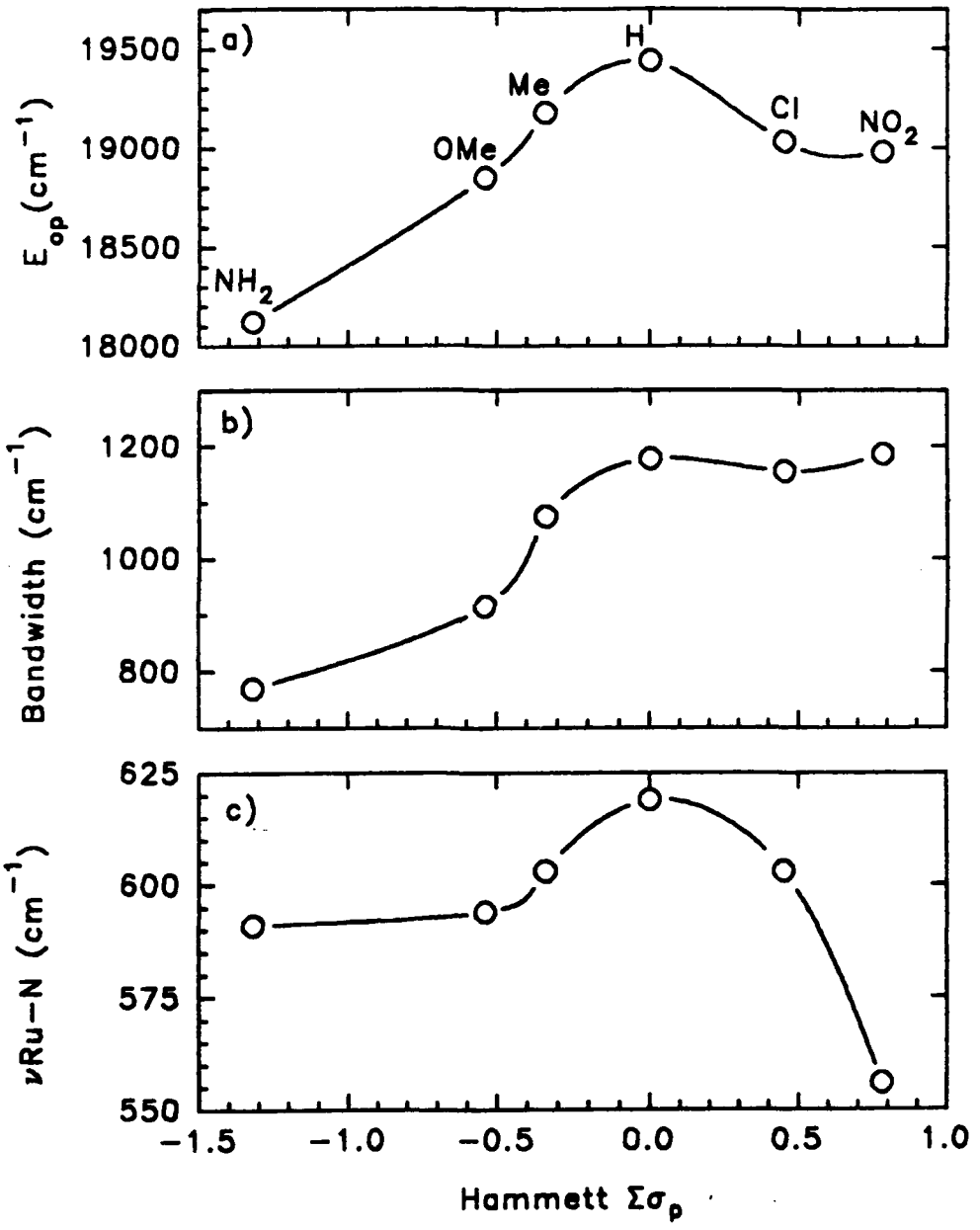
a)
b)
c)
E_{op} (cm^{-1})
Bandwidth (cm^{-1})
νRu–N (cm^{-1})
19500
19000
18500
18000
1200
1000
800
625
600
575
550
NH_2
OMe
Me
H
Cl
NO_2
−1.5
−1.0
−0.5
0.0
0.5
1.0
Hammett $\Sigma\sigma_p$